CHALMERS
UNIVERSITY OF TECHNOLOGY

Partial spider silk as scaffold for tissue engineering the aortic valve

Master thesis for fulfillment of the Master of Science Degree in Biomedical Engineering

CHRISTOS – PANAGIOTIS TASIOPOULOS

Department of Physics
CHALMERS UNIVERSITY OF TECHNOLOGY
Gothenburg, Sweden 2016

Partial Spider Silk as Scaffold for Tissue Engineering the Aortic Valve

CHRISTOS – PANAGIOTIS TASIOPOULOS

Department of Physics
CHALMERS UNIVERSITY OF TECHNOLOGY
Göteborg, Sweden 2016

Partial Spider Silk as Scaffold for Tissue Engineering the Aortic Valve

CHRISTOS – PANAGIOTIS TASIOPOULOS

Department of Physics

Chalmers University of Technology

SE-412 96 Göteborg

Sweden

Telephone + 46 (0)31-772 1000

The pertinent Master's thesis was conducted at the department of Protein Technology, School of Biotechnology, of Kungliga Tekniska Högskolan in collaboration with Spiber Technologies.

Cover:

Recombinantly synthesized spider silk assembled into fiber format.

Printed by Chalmers Reproservice

Göteborg, Sweden 2016

Abstract

The aortic valve constitutes a complex tissue that has to unobtrusively operate in a continuous mode, in order to sufficiently supply the systemic circulation with oxygenated blood. Severe aortic valve diseases though result in a tissue function no longer competent to meet the innately demanding biomechanical criteria. Conventional treatment approaches may temporarily alleviate symptomatic patients nonetheless have long been associated with great limitations. Tissue engineering holds great promise to cope with drawbacks of to date status in diseased aortic valve treatment, although has not been fully explored yet. Recombinantly synthesized spider silk has undoubtedly opened a wide range of application areas where sound mechanical properties are required and hence, it might be considered an ideal aortic valve scaffold. In this study, partial spider silk utilized to coat surfaces as well as configured into 3D matrices was extensively evaluated in terms of cell adherence, proliferation, and tissue-specific protein secretion. To provide comparable information, cell-seeded protein coatings and 3D constructs in the forms of foam and fiber were also exposed to vigorous fluid dynamics. Results indicated profound cell compliance with host material in general but most importantly, significant cell growth in the dynamically conditioned fibroblasts and endothelial cells inside the silk variants. In addition, protein-coated substrates and fabricated scaffolds subjected to shear stresses were interestingly shown to facilitate protein synthesis by seeded cells in a higher degree. In conclusion, recombinantly synthesized spider silk can be considerably included in future tissue engineering the aortic valve studies.

Keywords: Aortic valve tissue engineering, partial spider silk, scaffold, shear stresses

Contents

1 Introduction

Heart valves are considered the main regulators of unidirectional blood flow through the cardiac chambers and substantially, to the pulmonary and systemic circulation. In total, the heart contains four valves morphologically and functionally differencing one another. Tricuspid and mitral valves are collectively referred to as the atrioventricular valves due to be situated at the junctions between atria and ventricles. Despite sharing common functional traits, they differ in number of cusps as mitral valve is the only heart valve characterized by a two cusps configuration. On the contrary, the two semilunar valves, pulmonary and aortic, are located where blood exits the heart to lungs and aorta, respectively. They both share equal number of leaflets; though in rare cases, 1-2% [1], the aortic valve cusps are fused into two flaps as a consequence of congenital anomaly.

Valvular heart diseases although can potentially occur in any of the four heart valves, they have been reported to mostly affect either the mitral or aortic valve due to the higher developed pressures in left sided cardiac tissue [2,3]. They are hence the most common type of valves to be replaced and substitutes have to be met with certain criteria upon physician's decision. The current master thesis work however focuses mainly on the aortic valve with accompanying diseases and to date status of treatment.

1.1 Anatomy and physiology of the aortic valve

The aortic valve is located in a highly sophisticated macro- and micro-environment that allow the left ventricle to be emptied by the blood volume after each systolic phase of the cardiac cycle. Four inter-related, though morphologically different, components (Figure 1) are primarily involved in the aortic valve construct assembly; namely, the aortic annulus, the sinuses of Valsalva, the aortic cusps, and the sinotubular junction.

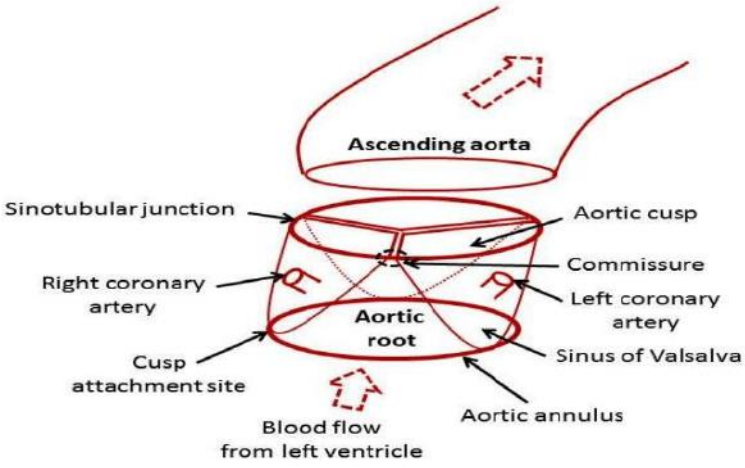

Figure 1 General overview of the aortic valve structure. The aortic valve conduit comprises the aortic annulus, the sinuses of Valsalva, the aortic cusps, and the sinotubular junction; assembling altogether the aortic root which is considered a separated part from the ascending aorta.

The aortic annulus is located at the junction between the left ventricle and the aortic root, structurally resembling to nearly a circular ring. The aortic cusps, attached to the annulus, are semi-lunar shaped and mainly participate in the orchestrated opening and closing function of the valve. The three adjoining areas between the aortic cusps and the sinotubular junction are known as commissures. The three sinuses of Valsalva constitute large and bulgy parts of the aortic wall and only two of them host the right and left coronary arteries responsible for the continuous supply of the cardiac sack with blood. The sinus lacking a coronary artery is known as the non-coronary sinus. At last, the sinotubular junction, a tubular shaped structure coupled with the sinuses, separates the aortic root from the ascending aorta [4].

In a normal function of the heart, the left ventricle is loaded with oxygenated blood in each diastole and pumps the blood towards the aorta in each systole. The key players in maintaining a coordinated opening and firmly sealing of the valve each time the heart beats are the cusps. Each of the three cusps is characterized by a three-layered structure, with each layer differently participating in the bifunctional behavior of the valve. Ventricularis is considered the bottom layer and closest to the left ventricle, hence the name, whereas fibrosa is the outermost layer facing the ascending aorta. The middle layer and thickest part of the cusp is known as spongiosa [4]. Each of the three layers is dissimilar in protein composition (Figure 2) and according to that fact, performs a unique function. Fibrosa is rich in circumferentially aligned collagen type I and III fibrils responsible for bearing the loads and stresses every time the orifice needs to open. On the contrary, radially oriented elastin sheets solely found on ventricularis are the main participants in tightly shutting the cusps and returning collagen fibrils back to relaxation state prior to each systole. Spongiosa is rich in glycosaminoglycans (GAGs) and provides all the necessary lubrication to ventricularis and fibrosa as they deform and crimp in each cardiac cycle. In addition, spongiosa acts as a shock absorber as well [5]. Hyaluronic acid (HA) and chondroitin sulfate account to a percentage of roughly 90% of the total amount of GAGs present on the human aortic valve [6]. The content of a native aortic valve in extracellular matrix (ECM) components accounts by approximation to: 60% of collagen, 30% of GAGs and 10% of elastin [7].

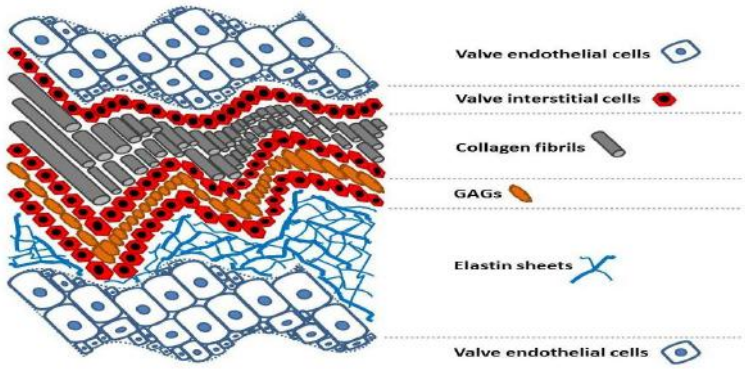

Figure 2 The anatomy of a three-layered aortic cusp. Fibrosa facing towards the ascending aorta is rich in collagen type I and III fibrils. Ventricularis locates at the bottom next to the left ventricle and contains mainly elastin sheets.

The middle part known as spongiosa provides all the lubrication and shock absorption via the abundant in GAGs deposits.

The cell types populating the aortic cusps are the valve endothelial (VECs) and valve interstitial cells (VICs), with the later displaying common morphological and functional features with fibroblasts, myofibroblasts, and smooth muscle cells [6]. Both cell types have developed a synergetic behavior by secretion of paracrine soluble factors, further ensuring the aortic valve's prosperity [8].

VICs are the most prevalent cell type met on heart valves and are involved in numerous functions according to their distinct phenotype. In total, five separate VIC phenotypes have been identified, namely: embryonic progenitor endothelial/mesenchymal, quiescent, activated, post-developmental/adult progenitor and osteoblastic VICs [9]. The activated VIC phenotype resembles more to the respective myofibroblast-like and is apparent all along the developmental and maturation stages of VICs. Activated VICs are highly associated with the cellular repair mechanisms, including cell proliferation and migration, and tissue remodeling. On the contrary, quiescent VICs display a more fibroblast-like phenotype and are largely related to maintaining the integrity and stability of the aortic valve by secreting the necessary ECM compounds. In their quiescent state, VICs express very low levels of α-smooth muscle actin nonetheless increased levels of vimentin as well, which are both strong and indicative biological markers to confirm the fibroblast-like phenotype [6,9]. At last, smooth muscle cells have been noticed to exhibit secretory as well as contractile phenotypic profiles, depending on their state of maturation. Less mature smooth muscle cells have been reported to participate in secretion of valve-specific ECM proteins together with fibroblasts, thereby preserving the aortic cusp micro-environment. In their most mature state however smooth muscle cells become contractile and are dispersed all over the distinct valvular layers, contributing in the opening and closing function of the cusps [4].

The second most common cell type populating the aortic valve, though in lesser amounts as compared to VICs, is the valve endothelial cells spanning all along the two distal surfaces of the cusp. The most significant role of VECs is to provide the anti-thrombogenic plateau next to the areas where leaflets come into contact with blood, in order to avoid thrombi formation. Additionally, VECs are involved in further driving immunological and inflammatory responses as they constitute the initial recognition site for incoming with the bloodstream signaling molecules as well as numerous growth factors [6]. Lately, VECs have been shown to differ from endothelial cells covering the rest of the cardiovasculature, as porcine endothelium tends to align perpendicularly to the direction of flow in contrast to endothelial cells in the aorta that are aligned in parallel to the shear stresses applied [9]. VECs are constantly exposed to flow pressures on both cusp sides though in different patterns and velocities. Endothelium on ventricularis experiences high shear-stresses and velocities from a laminar blood flow that results from supraventricular pressures

generated prior to each systole. On the contrary, VECs situated along the outermost side of fibrosa are exposed to lower shear-stresses and velocities induced by an oscillatory diastolic blood flow. As a result of the diverse shear stress intensities, VECs possess the ability to sense the alternating mechanical stimuli and translate them into corresponding biological responses significant for the longevity of each aortic valve layer, in a process known as mechanotransduction [4].

A native human aortic valve continuously supplies the systemic circulation with oxygenated blood and despite constantly accepting intense biomechanical stimuli, operates unobtrusively. As the ventricular pressure rises prior to each systole, a laminar shear stress is gradually applied to the cusps and pushes them to open. Consequently, blood is ejected towards the aorta and subsequently to the rest of the human body. On the contrary, oscillating blood vortices pooled in the interspace between the aortic walls and crimped cusps exert diastolic pressures, though significantly lower in magnitude to respective systolic, which force the leaflets to shut. To further elucidate the peculiar aortic valve function, Yap et al demonstrated that the shear stress applied to ventricularis ranges from 64 to 71 dynes/cm^2 at peak systolic pressure, in contrast to the respective exerted on fibrosa which estimated to peak at less than 20 dynes/cm^2, in two separate quantitative studies including native porcine and prosthetic aortic valves [10,11].

The uniqueness of the aortic valve operation therefore requires a pliable yet stiff at the same time tissue to compensate for the cardiac cycle's biphasic pressures. A comparative study conducted by Stradins et al on human cadaveric aortic valves indicated that the moduli of elasticity among the four main components assembling the aortic valve conduit insignificantly diversify (Table 1). A homogeneously flexible tissue can hence be assumed.

Table 1 Moduli of elasticity, E in MPa, of the main aortic valve elements as calculated on 11 cadaveric human aortic heart valves [12].

	Commissures	**Annulus**	**Sinotubular junction**	**Sinuses**
Modulus of elasticity (MPa ± SD)	13.80 ± 3.16	12.50 ± 2.98	7.41 ± 2.34	10.53 ± 3.22

The major fatigue though is experienced primarily by the aortic valve leaflets as collagen fibers on fibrosa have to continuously crimp with each systole, while elastin sheets on ventricularis radially stretch in each diastole to firmly close the orifice and prevent backflow. The anisotropic cusp milieu in protein composition and quantity thereby ensures a tissue portraying sound mechanical properties to sustain high compression and extension forces. A quantitative study performed by Balguid et al on 9 aortic valve leaflets as well as tissue engineered (TE) constructs under static and

dynamic straining shares a lot of insight regarding the tissue's mechanical properties [13]. The study involved the uniaxial tensile assessment of the aortic valve cusps in the circumferential and radial direction, in terms of modulus of elasticity, ultimate tensile strength, and strain at maximum stress (Table 2).

Table 2 Mechanical properties evaluated on 9 human aortic valve leaflets and tissue engineered constructs. Parameters calculated: (i) modulus of elasticity, E in MPa, (ii) ultimate tensile strength, σ_{max} in MPa, and (iii) strain at maximum stress, ϵ_{max} in %.

Specimen	Young's modulus (MPa)	Ultimate tensile strength (MPa)	Strain at maximum stress (%)
Native cusp (circumferential)	15	2.6	22
Native cusp (radial)	2	0.4	30
TE static	3	0.7	33
TE dynamic	6	0.9	25

The aforementioned parameters therefore suggest a complex tissue able to fully comply with the specific requirements dictated by the uninterrupted cardiac cycle. Nevertheless, the unique valvular mechanical properties might be greatly put at stake in cases of aortic valve diseases (AVD).

1.2 Aortic valve diseases

The most prevalent aortic valve diseases include either aortic stenosis (AS) or aortic regurgitation (AR). In a stenotic aortic valve, the leaflets become progressively calcified over time leading to partial opening as well as closing of the valvular orifice. The blood flow towards the aorta is eventually hampered. On the contrary, a regurgitating aortic valve results from an abnormal function of the bottom valvular parts, involving either the aortic root or annulus, or both, except for the cusps [14]. In both severe cases, the patient has to develop higher systolic pressures in order to compensate for either the partial opening or leaking blood, respectively.

Aortic stenosis. Followed by hypertension and coronary artery disease, aortic valve stenosis is the third most common cardiovascular disease met in the Western world [14]. The reasons driving to morbidity, which might ultimately lead to mortality were not be treated promptly, include the most notable risk factors afflicting the western individuals; namely: diabetes mellitus, hypertension, increased levels of low-density lipoprotein (LDL) cholesterol and lipoprotein (a), and smoking [15]. The human body's self-defense mechanism in AS is to initially deposit even more tissue around

the left ventricle in order to compensate for the higher systolic pressures, while simultaneously the left ventricle's chamber remains unaltered in volume capacity. The symptom is also known as concentric hypertrophy. The systolic pressure and valve function are nonetheless preserved, although not indefinitely. As the disease progresses, the systolic function collapses and blood flow towards the right and left coronary arteries starts declining even in healthy and fully operational pericardial arteries. Eventually, the patient risks passing away either from angina pectoris (35%), syncope (15%), or heart failure in general (50%) [16,17]. Both cell types populating the aortic valve leaflets are being significantly affected by a gradually degenerating environment and changes in their phenotypic profiles have been reported. VICs have been shown to acquire a more osteoblast-like phenotype under non-uniformly shear stresses applied and subsequently secret extra ECM components, thereby contributing in an ever increasing calcified tissue [18]. It has been noted by Mol et al that VICs expressing pro-inflammatory cytokines by themselves under abnormal aortic valve function mediate in altering their phenotypic profile to a more osteoblast-like [19]. On the other hand, VECs not accustomed to non-canonical systolic and diastolic pressure patterns than that normally experiencing become less resistant to fatigue. As a consequence of the induced to endothelium wear and tear, degenerative lesions are highly likely to occur and thus the affected surface of the cusp retains no longer its non-thrombogenic properties. In addition, the levels of calcification inhibitory proteins naturally expressed by VECs are significantly decreased when aortic valve undergoes stenosis [8].

Aortic regurgitation. In contrast to stenosis, a more complex and broad variety of valve abnormalities and cusps dysfunction may gradually result in aortic valve regurgitation. So far, rheumatic heart disease was the prime factor leading to AR. Evolving diseases linked with the ascending aorta and aortic root however have been recently reckoned by the medical society to more often cause AR in the developed countries [14]. Additionally, numerous congenital aortic valve deficiencies, in particular fused to bicuspid or unicuspid valves, quadricuspid valves, and valves with fused commissures, as well as acquired ones, i.e. aortic cusps retraction due to fibrosis and infective endocarditis, have been to a lesser or greater extent associated with AR [15]. In essence, aortic regurgitation describes the irregularity where blood parts of the stroke volume flow in reverse direction, from the ascending aorta back to the ventricle, upon applied diastolic pressures. The deficiently operating valve is the result of a failing to retain higher pressures than that of the aorta's side left ventricle and therefore, the valvular orifice fails to completely shut. Unavoidably, the left ventricle becomes overloaded as reversely flowing blood joins with incoming stream from lungs. At early stages of AR, myocytes populating the cardiac tissue are gradually elongated to form an extensive fibrotic network around the left ventricle, in an attempt to dilate the chamber and facilitate the ejection of pooled blood volumes [14]. This particular self-defense mechanism is also known as eccentric hypertrophy. Eccentric as well as concentric hypertrophy stemming from the elevated left

ventricular pressures due to overloads aid maintaining a normal systolic function and therefore, patients remain asymptomatic for long time [17]. As AR progresses though, the repeatedly uneven loading and unloading results in a collapsing systolic function and subsequent increased end-diastolic pressures in the left ventricle. Patients may suffer among others from shortness in breath on exertion initially but even when lying down in acute AR, paroxysmal nocturnal dyspnea, and angina pectoris as blood flow to left and right coronary arteries reduces [20]. Aortic valve replacement (AVR) therefore may significantly improve the systolic function by restoring chamber's loading volumes to normal figures and alleviate AR patients, were to be carried out as early as possible.

1.3 Conventional aortic valve treatment

Heart valve replacement operations account to approximately 280.000 surgical procedures all over the world annually [21]. In Sweden, about 300 incidents each year are solely operated at Sahlgrenska University Hospital in Göteborg [22]. Aortic valve is the most common valvular type to be replaced worldwide and estimated to reach more than 200.000 procedures each year [23]. The Swedeheart annual report issued in 2014 announced that in Sweden isolated aortic valve replacements ranged from 700 to 950 incidents between years 2003 – 2013 [24]. In general, deficiently operating aortic valves are being replaced by either a mechanical or bioprosthetic equivalent. The diverse bioprosthetic valves are either of animal origin, mainly porcine or bovine, or human donated, such as in the cases of using a homograft, which is also known as allograft. Due to favorable hemodynamics and identical conformation, a diseased aortic valve can be also substituted with patient's own pulmonary in a surgical operation known as Ross procedure [25]. Lately, a novel approach that gains an ever increasing interest among the medical society and followed primarily in severe AS cases is the transcatheter aortic valve replacement (TAVR). The choice of the most desirable prosthesis though as well as technique relies upon specific criteria defined by the physician in charge and usually include the patient's age and overall health condition, the severity of disease, and patient's ability to permanently follow anti-coagulant medication.

Mechanical valves. In total, three basic types of mechanical valves are available and more precisely, monoleaflet, bileaflet, and caged ball valves [21]. Nonetheless, caged ball replacements are no longer implanted due to high susceptibility in blood clotting and damaging cells circulating with the bloodstream [6]. Mechanical valves are generally fabricated of pyrolytic carbon and polyester materials and are diametrically covered by a soft textile made of expanded polytetrafluoroethylene (ePTFE) where the cardiac surgeon sutures the stiches to keep the valve in place. Monoleaflet valve as the name suggests employs a single leaf that partially opens at an angle of 60° to 80° degrees approximately, thereby resulting in two differently sized valvular apertures. On the other hand, bileaflet valves consist of two semi-lunar shaped disks that open to about 90° degrees and allow blood to flow towards the aorta through the

three unequally sized spaces created [21]. Mechanical valves despite being long lasting and resistant to wear and tear have been widely associated with thrombus formation and subsequent thromboembolic complications, as well as hemorrhagic events due to the unavoidable uptake of anti-coagulant medication by the patient [26]. In addition, patients wearing a mechanical valve often complain about a clicking sound produced as the valvular orifice closes; although the exact pathophysiological reasons leading to the sound are not fully comprehensible yet [27].

Bioprosthetic valves. Initially, bioprosthetic valves which are also known as biological valves were stented and glutaraldehyde crosslinked, retaining a shape identical to that of a native aortic valve's; albeit of porcine origin. Moreover, pericardial valves mounted on a supporting stent as well and entirely made of three bovine pericardium pieces served as an alternative option to porcine. Nevertheless, poor hemodynamics primarily and break susceptibility secondarily led to designing stentless aortic valve replacements of same species [21]. On both cases though, bioprostheses have to be treated with glutaraldehyde in low concentrations as well as other chemicals to reduce rejection rates and increase resistance to calcification while implantation, respectively [28]. Homografts are human origin tissues and the most rarely biological valve types to be implanted due to shortage in donors. They are protocol accordingly cryopreserved and stored until use, containing the entire aortic root and in few cases the ascending aorta as well [29]. Bioprosthetic valves in general do not require an anti-coagulant medication to be taken by the recipient and thereby, thromboembolic complications are extremely seldom to occur; less than 2% each year [6]. The life expectancy though of bioprosthetic valves is considerably low as compared to the mechanical equivalents with an average lifetime estimated to be hardly 15 years [30]. As a consequence of poor durability, 65% of patients wearing a bioprosthetic valve and less than 60 years of old need to be inevitably re-operated [6].

Ross procedure. The Ross procedure conceived and firstly implemented by Dr. Donald Ross in 1967 involves the removal and re-implantation of patient's own pulmonary valve in the aortic place and the subsequent implantation of a cadaveric homograft in place of the absent pulmonary valve [28]. Replacing diseased aortic valve with patient's own pulmonary favors infants and children with fused aortic valve cusps or related congenital abnormalities, as the pulmonary valve grows naturally alongside patient; though has long been debated in adults [31]. Furthermore, Ross procedure is generally described as an intricate surgical operation requiring a highly skillful cardiac surgeon in charge and in addition, 20% of patients would be unavoidably needed to re-operated 10 years after the initial surgery [6].

Transcatheter aortic valve replacement. This approach similarly to stenting procedures employs a catheter inserted in the human body through a minimally performed incision and upon which the aortic valve replacement is mounted. So far, several insertion sites have been tried with the most popular being the transfemoral and transapical areas. Once the catheter has reached the stenotic valve location, a

balloon around which the stented prosthesis is tightly coiled is inflated and pushes the stent to open. Subsequently, the balloon is deflated and removed while the aortic valve prosthesis remains in place. TAVR has been developed to treat elderly as well as patients belonging to high-risk subpopulations vulnerable to post-operational complications, should be conventionally (AVR) operated. According to Assadi et al, those particular subpopulations include patients suffering from either one or more of the following: systolic heart failure or coronary artery disease, cerebrovascular and peripheral artery disease, chronic kidney disease, and chronic respiratory function, except for severe aortic valve stenosis [32]. TAVR related embolic events in the carotid or vertebral arteries have been nonetheless reported as a consequence of atherothrombotic particles dislodged from plaques covering the vessels through which the catheter travels towards the aortic root [32].

1.4 Tissue engineering approaches

Tissue engineering (TE) approaches although not fully explored yet hold great promise to deal with scarcities of conventional AVR treatments and alleviate patients permanently. Despite the different concepts studied, the rationale behind tissue engineering a heart valve (TEHV) or any other organ involves a scaffold to serve as the substrate and tissue-specific cells to be seeded into it. In addition, the complex system scaffold-cells often has to be cultivated in a highly specific physicochemical environment that as much as possible mimics the conditions experienced by cells in vivo.

Scaffolds for heart valve tissue engineering approaches. An ideal scaffold should be designated by general specifications, collectively referred to as: (i) adequate mechanical properties for the application area, (ii) non-cytotoxicity, thereby facilitating cell viability and proliferation, (iii) gradual degradation after insertion to human body, and finally (iv) biocompatibility with surrounding host tissue to not initiate immune responses [28]. Scaffolds that have been extensively used in TE applications can be classified into two main groups: natural and synthetic. Natural scaffolds can be either decellularized ECM tissues, frequently of porcine origin, which have been purified from cellular components and debris prior to use, or native proteins, such as collagen, elastin, hyaluronic acid, fibrin and fibronectin [33], for instance. On the contrary, a broad range of artificially made materials, most commonly bioresorbable polymers, have been to a lesser or greater extent evaluated as potential aortic valve scaffolds. The most notable polymers used so far in TEHV studies include: the poly-lactic and poly-glycolic acid (PLA and PGA, respectively), poly-L-lactide (PLLA), and poly-caprolactone (PCL), as well as composite materials composed of either one of those polymers and added agents, i.e. poly (4-hydroxybutyrate) with PLA or PGA, or mixed together, such as PGA/PLLA [6].

Decellularized porcine ECM scaffolds studied in TEHV applications have shown reduced calcification levels in comparison to bioprosthetic valves, non-cytotoxicity,

and retained mechanical properties if not treated with harsh detergents [34]. On the other hand, they have been reported by Kasimir et al as platelet-activating surfaces and thereby, thromboembolic events may subsequently occur; though significantly less if matrices are seeded with endothelial cells [35]. Additionally, enzymatic decellularization with deoxyribonuclease (DNase) or ribonuclease (RNase), spit freezing and radiation, as well as use of strong enzymes or detergents, i.e. more than 0.5% trypsin and ammonium hydroxide, led to significant deterioration of the structural components and compromised mechanical properties, as adventitial collagen became less condensed and space between the fibrils increased [6].

On the contrary, native proteins such as collagen type I and elastin used as scaffolds have shown sound consistency due to inherent mechanical properties, adequate compliance with host tissue, and low induced immunogenicity [36,37]. Collagen type I nevertheless requires either crosslinking with an additive agent, i.e. pentagalloyl glucose, or blending with a polymer, as it exhibits quicker degradation profiles than desired [38]. Faster degradation time may potentially put at risk the entire scaffold's as well as host tissue's integrity, should cells repopulating neighboring area have not managed to deposit adequate amount of structural components. On the other hand, elastin has been associated with calcification when used as a biomaterial and may act as a nucleation site leading to mineralization as well [6].

Lastly, synthetic materials in general can be easily engineered in terms of stability, gradual degradation rate, and porous interconnectivity, as well as rapidly scaled up. Nonetheless, they are usually made of resorbable polymers difficult to control cell adhesion and often accused of entrapping deep inside the matrices cells that do not have access to nutrients and oxygen and thereby led to apoptosis. Additionally, inflammation might be induced due to leaking particles degrading faster than the polymer as a whole [39]. Out of the various artificially made biomaterials studied, PGA and PLA have been extensively used as TE scaffolds due to be the only FDA approved materials for further implantation in the US [28]. As a matter of fact though, PGA, PLA and composite materials derived from them have been reported as poor substrates for in vitro cell growth [40].

Cell sources for heart valve tissue engineering approaches. Cells to be seeded into scaffolds are a key parameter in TE applications as well and so far, diverse cell types and sources have been largely assessed in terms of cell survival, proliferation, differentiation, and ultimately maturation. Cell sources are classified into three main groups and include: xenogeneic, i.e. cells derived from animal species, allogeneic, i.e. human donated cells, and finally, autologous cells, i.e. cells isolated from the same patient though different tissue [8]. The most commonly used cell types include: dermal or foreskin fibroblasts, isolated aortic myofibroblasts as well as endothelial cells from native aortic leaflets, marrow stromal cells, human umbilical vein endothelial cells (hUVECs), and umbilical cord myofibroblasts [41]. Lately, a lot of

focus has been put on making use of stem cells in TEHV applications and more precisely, either endothelial progenitor (EPCs) or mesenchymal stem cells (MSCs) found primarily on the bone marrow. Both can be very easily extracted and do not fall into strict ethical permissions as compared to embryonic stem cells [33].

Xenogeneic cell sources include mainly cells of porcine, bovine, ovine, and caprine origin. They are usually off-the-shelf, inexpensive, and less ethically restricted in use as compared to the respective of human origin. Further, animal derived cell types display similar phenotypes to respective human ones, constituting xenogeneic cell sources highly popular for in vitro and preclinical studies. Cells isolated from animal species though have been related to contamination, as numerous diseases can be very easily transmitted and moreover, initiate immune responses to hosts in vivo [8].

Allogeneic and autologous cells are both human derived with the difference being that allogeneic have to be either donated or isolated from a cadaver. Allogeneic cells are therefore highly likely to invoke immunogenicity with subsequent graft rejection and as a result, the recipient should be constantly treated with immunosuppressive medication. On the other hand, a comparative study conducted by Smith et al demonstrated that human isolated interstitial cells exhibit sound biomechanical properties when seeded into 3D collagen matrices, posing them good candidates for TEHV applications [42]. Autologous cells in contrast, despite not initiating immune responses post-operationally, are not a competent cell source to treat overaged patients or patients suffering from side cardiac diseases, except for the related to the aortic valve [8].

Fibroblasts, either dermal or foreskin, have been widely utilized in tissue engineering approaches in general, as they can be very easily isolated, expanded, and synthesize valuable ECM components; especially collagen and GAGs. Additionally, it has been shown that fibroblasts when treated with the transforming growth factor β (TGF-β) differentiate into myofibroblasts and therefore regenerate cardiac tissues [43]. Human foreskin fibroblasts have been also shown to successfully cooperate with hUVECs in vitro in a model study aiming to form oriented vessel-like structures between adjacent monofilaments [44]. Fibroblasts can hence be assumed a highly indicative cell type for further exploitation in tissue engineering the aortic valve.

The endothelium covering the umbilical cord veins is a highly rich source for extracting hUVECs that have been broadly used in model studies of the cardiovascular system. Endothelial cells from umbilical veins provide the antithrombogenic milieu necessary to avoid thrombi formation as well as secrete the indispensable structural proteins, i.e. elastin, to render TE constructs pliable [8]. Weymann et al succeeded to entirely decellularize human pulmonary and aortic allografts, though retaining their mechanical properties, and re-cellularize them with isolated and in vitro expanded hUVECs. Results indicated a confluent cell monolayer

of hUVECs which were positively labeled for von Willebrand factor and CD 31 marker, thereby confirming their endothelial phenotype [45]. Endothelial cells isolated from umbilical veins can thus be regarded a competent cell source in tissue engineering valvular constructs.

A relatively novel alternative as a cell source in TEHV is the use of stem cells that are primarily located in the bone marrow and more precisely known as hematopoietic, endothelial progenitor, and mesenchymal stem cells. The most extensively stem cells used are the endothelial progenitors that differentiate into endothelial cells spanning all along the cardiovasculature and mesenchymal that form muscles likewise heart among others. EPCs provide all the necessary elasticity required in tissue engineering a heart valve and vasculatures in general and in addition, they succeed in maintaining anti-thrombogenicity [46]. MSCs are a much welcoming cell source in TE, as they can be easily isolated from numerous human body sites, including: the bone marrow, adipose tissue, peripheral blood, umbilical cord blood and matrix, amniotic fluid, and chorionic villi, and differentiate into various cell types under the proper physicochemical conditions [47]. Two quantitative studies involving MSCs seeded into a bio-resorbable polymeric scaffold and decellularized porcine valves respectively reported the detection of indicative biological markers, such as α-smooth muscle actin (αSMA), vimentin, myosin heavy chain, and desmin, confirming the successful differentiation into myofibroblasts in a phenotypic analysis performed [48,49]. Nevertheless, a major limitation when using pluripotent stem cells as a cell source in tissue engineering is often the accompanied risk in teratomas formation.

Conditioning of cell-seeded scaffolds in heart valve tissue engineering approaches. The native environment in which an aortic valve lies provides unique physicochemical properties that allow the valve to thrive and unobtrusively operate. A great need is therefore required to more accurately design TEHV applications able to mimic the specific conditions ex vivo. A plethora of systems have been implemented throughout the various concepts studied, including merely a rocking platform to produce fluid shear stresses in the simplest of notions up to tailor-made bioreactors that subject TE constructs in perfusion pressures. In any case, the seeded scaffold is conditioned under solid sterilization provided by an incubator that also allows monitoring of vital signs, such as temperature and CO_2 levels.

In an effort to validate the physical and biological stimuli experienced by cells under fluid shear stresses, Tucker et al reported agreement between computationally obtained and experimentally measured velocity values when fluid stimulation was generated by a see-saw rocking system. Maximum shear stress values could be subsequently computed across the entire surface of the culturing well, thereby dictating where the most intense forces are applied upon cell culture surfaces in similar setups. In addition, human tenocytes put under the dynamic conditions

generated by the system displayed significantly increased collagen and GAGs secretion at pre-defined culture time points [50].

A novel bioreactor tailor-made to pumping culture medium in a pulsatile mode was utilized by Aleksieva et al to experience endothelial cells and fibroblasts under perfusion pressures. Cells were isolated from saphenous vein segments and seeded into polyurethane scaffolds. Scanning electron microscopy results of the two cell groups cultured under static and dynamic conditions indicated adequate cell adherence on both cases; though better cell dispersion and behavior on the later. In addition, immunohistochemistry evaluation of stained cells within the matrices showed higher expression of collagen type IV and intracellular adhesion molecule in the dynamically conditioned cell-seeded scaffolds, suggesting cell tolerance to shear stresses [51].

A more sophisticated system was developed by Sun et al to condition porcine aortic valve leaflets under side-specific shear stresses. The double cone-and-plate device was capable of delivering perfusion pressures in different intensities on each side of the mounted tissue samples. After 4 days of culturing period, immunohistochemistry assessment indicated no significant alteration in endothelial integrity and cellular apoptosis between the dynamically conditioned specimens and controls [52]. The said study validated the dual nature of endothelial cells covering the two distal sides of the aortic cusp and can be further exploited in studying the reasons underlying aortic valve calcification.

So far, approaches to tissue engineer the heart valve have demonstrated promising results further enlightening the field and more precisely, where the future research should be focused. Nevertheless, numerous bio-fabricated constructs seeded with cells fail to fully function in the long term, as they are no longer complied with some of the specifications that should be designating a solid scaffold. In general, the uneven distribution as well as poor secretion of extracellular matrix components has been recognized to lead to compromised mechanical properties in TEHV implementations [28,39]. Consequently, artificially made valvular prototypes often fail to retain a similar shape and function to that of a native's aortic valve.

In addition, elastin despite found in lesser amounts as compared to the rest of the ECM building blocks plays a significant role in maintaining the equilibrium between cardiac cycles and tightly shut the leaflets after each systole. Absence in elastin deposition has long been reported in applications aiming to tissue engineer the cardiovasculature [19,53]. One can understand hence that elastin might be the key in further improving the current tissue engineering approaches, given a sound material to support cell maturation.

1.5 Partial spider silk

One such biomaterial holding promise to be used in tissue engineering the cardiovasculature and the aortic valve precisely is the partial spider silk. Natural spider silk is a remarkably strong yet pliable biomaterial though rather hard to be collected from webs, as it is a time-consuming process [54]. In addition, the predatory behavior that spiders develop when kept under captivity do not allow large scale production of natural silk [55]. Biotechnological approaches have therefore led to recombinantly engineer spider silk that can be expressed by various hosts, including bacteria, i.e. Escherichia coli (E.coli), yeast, plants, and mammalian cell lines among others [54].

To recombinantly synthesize partial spider silk, a lot of intermediate steps are involved in a complex process that ultimately yields the end-purified-protein. The entire process includes the following important steps: (i) full length cDNA isolation that codes for silk protein assembly in spiders, (ii) isolation of cDNA that specifically codes for partial spider silk, (iii) cleavage and subsequent insertion of cDNA to a target vector, (iv) transformation of the recombinantly engineered DNA (rDNA) into the host, (v) expression of rDNA, and finally (vi) silk protein harvesting and protein purification by usually following an affinity purification protocol [54,56].

To be further used in TE applications, the silk protein can be configured into several different formats that serve as matrices able to be seeded with various cell types. Spider silk biomaterial has been extensively studied as a potential TE scaffold and casted among others into films [57-59], microbeads [60], and microspheres [61,62]. Furthermore, salt leaching techniques have been implemented as well [63] in an effort to constitute silk-based scaffolds more porous interconnected networks. Lately, recombinantly engineered spider silk has been also except for film successfully configured into mesh, fiber, and foam formats [64] with sound physicochemical properties [56, 65, 66].

Dragline silk exceptionally known for its unique mechanical properties in terms of tensile strength and ductility [67] is composed of two proteins that dispose similar amino acid sequences. The proteins are also known as major ampullate spidroins 1 and 2 (MaSp1 and MaSp2, respectively) [68]. The intermediate region between the non-repetitive N- and C-terminal domains that account approximately 100 - 150 amino acids each contains highly recurrent poly-alanine sections discontinued by glycine-rich repeats [65]. The long repetitive sequence between the two terminal domains is the key element for the remarkable mechanical properties. Stark et al managed to shorten the MaSp1 protein into a fragment containing a mere sequence of four poly-alanine / glycine-rich repeats and the C-terminus, known as 4RepCT [56]. The protein was subsequently assembled into fibers and tested for its mechanical properties along with three mutant fibers [65] (Table 3). Mutants were synthesized by

using 4RepCT as the template and introducing disulfide bridges between the poly-alanine segments, CC_1, CC_2, and S.

Table 3 Mean maximum stress, σ_{max} in MPa, mean maximum strain, ϵ_{max} in %, and mean initial modulus, E in GPa, as calculated on 4RepCT and two mutant fibers [65].

Protein	Mean maximum stress (MPa) ± SD	Mean maximum strain (%) ± SD	Mean initial modulus (GPa) ± SD
4RepCT	80 ± 20	1.0 ± 0.1	9 ± 2
CC_1	110 ± 30	1.2 ± 0.3	12 ± 4
S	80 ± 30	0.9 ± 0.2	10 ± 4

Results indicated sound mechanical properties on 4RepCT fibers that can be further improved by introduction of mutagens into the main sequence. Nevertheless, figures related to solely the 4RepCT protein display a tough yet flexible silk-based material, showing great potential to tissue engineer the cardiovasculature.

An ideal scaffold to be used in TE applications should preferably be capable of acting as an attraction site to tissue-specific cells in vitro as well as in vivo post implantation. The tripeptide RGD (arginyl-glycyl-aspartic acid) motif found primarily on fibronectin has been covalently introduced to proteins expressed by heterologous hosts, including partial spider silk [69,70], in order to improve cell attachment and proliferation [58]. Widhe et al succeeded to genetically incorporate the RGD motif, among others, into the 4RepCT mini-spindroin and configure the functionalized protein into fibers, foams, and films [70]. Results indicated an improved cell adherence and satisfactory growth rate of human dermal fibroblasts in the RGD-coupled protein as compared to the wild type version (4RepCT) and the negative non-functional RGE control motif. In a more recent study [71], partial spider silk was successfully coupled with a fibronectin mimetic motif and efficiently assembled into stable film formats. The functionalized silk (FN-4RepCT) with the RGD motif as a turn loop stabilized by cysteines displayed sound cell adherence of human primary cells as well as profoundly supported proliferation and migration of adhered keratinocytes. Lately, Jansson et al have shown that 4RepCT can be successfully functionalized with even more affinity domains by implementing gene fusion technology and assembled into chemically and thermally stable film and fiber formats [72].

So far, recombinant spider silk has unfortunately been little evaluated in vivo in terms of biocompatibility to host tissue for the application areas implanted. Porous membrane formats of partial spider silk have been studied by Baoyong et al as wound dressings on deep burns in mice and results reported a considerable wound healing

promotion, in the same way as collagen sponges do in clinical use [73]. In another in vivo study conducted by Fredriksson et al, fiber bundles made of the 4RepCT protein were subcutaneously inserted into rat models and subjected to histological assessment one week post-operationally. Formation of new capillaries as well as ingrowth of fibroblasts around the implants was observed though few foreign body giant cells (FBGCs) signifying inflammation were reported as well [74].

Taken altogether, recombinantly synthesized spider silk designates a solid biomaterial fulfilling to a lesser or greater extent the requirements that should be describing an ideal scaffold to be used in tissue engineering the heart valve.

1.6 Aim of the study

The aim of the current study is to as highly as possible attempt to address the aforementioned limitations with regards to recent tissue engineering the aortic valve approaches by making use of a relatively novel biomaterial. More specifically, partial spider silk in various formats was concisely examined as the aortic valve scaffold to support cell adherence, viability, proliferation, and ultimately maturation.

1.7 Study overview

To as concretely as possible evaluate the potential of partial spider silk used as the substrate, coatings with the protein as well as matrices in the forms of foam and fiber were seeded with two separate cell types and subjected to static and dynamic conditions. The material used in the experimental setup involved the wild type 4RepCT (from now on denoted WT) as well as the respective functionalized FN-4RepCT (from now on denoted FN) of the partial spider silk protein. The two cell types expanded and used throughout the entire experimentation were the human umbilical vein endothelial cells and human neonatal dermal fibroblasts (hDFn).

Fluid shear stresses generated by a wave-rocking platform entirely made of lego® pieces (from now on referred to as lego-vagga) aid dynamically condition cells on protein coatings as well as 3D scaffolds. To be compared with, they were also put under static conditions by simply let to grow at 37 °C with 5% CO_2 and 95% humidity.

The experimental approach was divided into three chronologically separate among them phases. Initially, hDFn were seeded onto protein coatings and kept in culture on both conditions for 8 days. Later, hUVECs were subjected to the exact same process though 14 days instead. The second phase of the experimentation involved the preparation of cell-seeded constructs in forms of foam and fiber and their subsequent expansion for 14 days under both the static and dynamic conditions. Finally, the last part involved the optimized process of conditioning the cell-seeded fibers solely.

Cell viability and growth rate data in parallel with quantification analysis results processed from the captured immunofluorescence images served as a comparison yardstick between the two anisotropically conditioned cell types.

2 Materials and methods

2.1 Lego-vagga configuration

In a study aiming to quantify fluid shear stress in a rocking culture dish, Zhou et al proposed that the maximally generated fluid shear stress is inversely proportional to the squared factor δ, which is the fraction of culture medium height on the dish over its respective diameter [75]. The fluid shear stress is also dependent on the rocking frequency (f) as well as maximal flip angle (θ_{max}) and can be calculated by the following formula:

$$\tau_w = \frac{3 \cdot \pi \cdot \mu \cdot \theta_{max}}{4 \cdot \delta^2} \cdot f$$

The μ value represents the viscosity of culture medium and equals to 0.0078 dynes·sec/cm^2 [76,77]. Given that the maximum rocking frequency that the power-supply unit (Velleman Inc, Fort Worth, US) could provide at 9V was 4.58 cycles/sec and maximal flip angle (θ_{max}) that the lego-vagga (Figure 3) could reach was 6°, the calculated by approximation maximum shear stress was therefore equal to 22.45 dynes/cm^2. It was considered nevertheless sufficiently enough to experience cells in vigorous fluid dynamics.

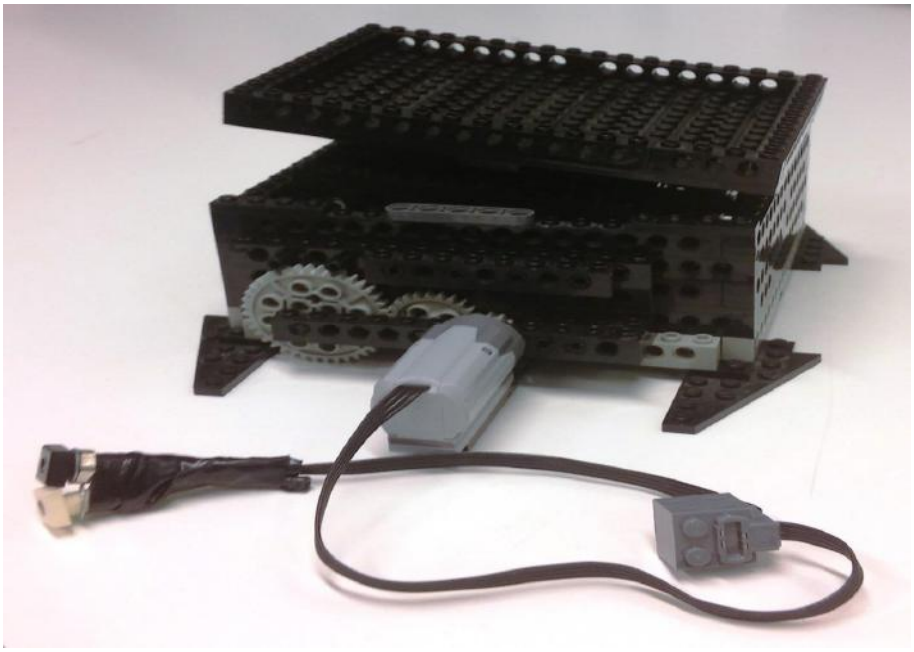

Figure 3 The lego-vagga wave-rocking platform used to dynamically condition hDFn and hUVECs seeded onto protein-coated surfaces as well as into 3D matrices. It occupies a single platform that can perfectly host a 24-well

plate and two positive and negative sockets to be connected with a power supply unit. The power motor unit (grey piece) can withstand ac currents up to 9V.

The rocking frequency (speed) to fibroblasts seeded onto protein coatings and kept in culture for 8 days was changed approximately every second day (Table 4). On the contrary, settings were changed every four days to endothelial cells seeded onto protein coatings as well as fibroblasts and endothelial cells seeded into 3D matrices (Table 5). Both were kept in expansion for 14 days.

Table 4 Lego-vagga settings in hDFn seeded onto protein coatings and cultured for 8 days.

Days in expansion	Power-supply unit voltage (V)	Rocking frequency (cycles/sec)	Fluid shear stress (dynes/cm^2)
Day 1	+2	1.02	5
Day 3	+4	2.04	10
Day 6	+8	4.08	20

Table 5 Lego-vagga settings in hUVECs seeded onto protein coatings as well as hDFn and hUVECs into 3D matrices. Both were kept in expansion for 14 days.

Days in expansion	Power-supply unit voltage (V)	Rocking frequency (cycles/sec)	Fluid shear stress (dynes/cm^2)
Day 2	+2	1.02	5
Day 6	+4	2.04	10
Day 10	+8	4.08	20

2.2 Cell culture

Endothelial cells. Primary human umbilical vein endothelial cells isolated from the vein of a single donor's umbilical cord (PromoCell, Heidelberg, Germany) were cultured at passage 3 in basal endothelial cell growth medium (PromoCell) supplemented with the endothelial cell growth medium supplement mix (PromoCell). Cells were plated in pre-coated T-75 flasks (Sarstedt, Nümbrecht, Germany) with 3 mL 0.1% gelatin (Sigma-Aldrich, St. Louis, US) to allow better cell adherence and kept in expansion for 7 days after thawing. The seeding density in the flasks was 5000 cells/cm^2, according to manufacturer recommendations. When necessary, cells were passaged upon reaching 80 - 90% confluency. In all the experiments performed, the used hUVECs were between passages 4 and 6, and the growth medium was changed every second day.

Fibroblasts. Primary human neonatal dermal fibroblasts isolated from juvenile foreskin (PromoCell) were cultured at passage 6 in Dulbecco's modified eagle's medium / nutrient mixture F-12 Ham (Sigma-Aldrich) supplemented with 5% fetal bovine serum (FBS) (Gibco, Paisley, UK) and 1% PEST. Cells were plated in T-75 flasks and kept in expansion for 7 days after thawing. The seeding density was exactly the same as with hUVECs, namely 5000 cells/cm^2. Fibroblasts were also passaged upon reaching 80 - 90% confluency and all the experiments were conducted between passages 7 and 9. Growth medium was changed every second day as well.

2.3 Preparation of protein coatings

In details, the protein (generously provided by Spiber Technologies AB, Stockholm, Sweden) was initially thawed at room temperature and subsequently spun down for a minute using a bench top centrifuge. The protein was then extracted from the supernatant and diluted in 20 mM Tris-HCl (pH 8.0) buffer to a concentration of 0.1 mg/mL. Super ultra-hydrophobic cover slips of 12 mm in diameter (Paul Marienfeld, Lauda Königshofen, Germany) were beforehand autoclaved and placed where necessary in the wells of a 24-well plate. The cover slips served to capture better quality immunofluorescence images under the microscope. Further, the dissolved protein was pipetted on top of the cover slips and coated surfaces were let to incubate for 60 minutes at room temperature with the lid of the 24-well plate on. Once the incubation time was completed, the protein solution was removed and cover slips were washed twice with 20 mM Tris-HCl (pH 8.0) buffer. They were then left to dry for a few seconds and 100 µL of 20 mM Tris-HCl (pH 8.0) buffer was added at last. The plate was sealed with parafilm and stored at 4 °C.

2.4 Cell-seeding onto protein-coated cover slips

Initially, hDFn and hUVECs kept in expansion were harvested according to typically followed protocols in cell culturing. Briefly, growth medium was aspirated from the flasks and cells were washed once with phosphate-buffered saline (PBS). Cells were enzymatically detached by adding TrypLE™ (Thermo Fischer Scientific, Waltham, US) into the flasks and let to incubate at 37 °C with 5% CO_2 for 10 minutes. Cells were then checked under the microscope whether they have detached and counted with trypan blue in a Bürker chamber. Harvested cells were subsequently prepared in a cell suspension of 10^6 cells/mL containing the respective media. Further, cells were diluted accordingly in order to yield for each cover slip a final seeding density of 3000 cells/cm^2. Once the final cell suspension was prepared, a 100 µL was pipetted on top of each pre-coated cover slip as well as to non-pre-coated ones ($n = 2$) that served as negative controls. At last, pre-warmed at 37 °C growth medium was added to the wells and cells let to adhere overnight.

2.5 Preparation of protein-made cell-seeded 3D scaffolds

Fibers. Cells in expansion were harvested as described above and prepared in a cell solution of 10^6 cells/mL containing respective growth media with 1% HEPES (4-(2-hydroxyethyl)-1-piperazineethanesulfonic acid) and no FBS. Once the FN protein was thawed at room temperature, it was carefully mixed with harvested cells in respective growth media inside tubes. Tubes were then let to tilt on a tilting table at room temperature for 3 hours in slow mode. Once the incubation time was completed, the tubes were gently shaken to allow fiber detachment from the walls. Fibers were then transferred to a petri dish (Sarstedt) containing pre-warmed at 37 °C PBS with a beforehand autoclaved dentist-tool. Using a disposable scalpel (Swann-Morton, Sheffield, England), fibers destined to be dynamically conditioned were cut to roughly 2 – 3 cm pieces long and mounted in pairs on culture-inserts (Ibidi, Martinsried, Germany). Culture-inserts with mounted fibers (Figure 4) were subsequently transferred to a 24-well plate and respective media was added and changed every second day. Cell-seeded fibers destined for static conditioning were normally cultured in a 24-well plate at 37 °C with 5% CO_2 and 95% humidity.

In the optimized experimental setup, cell-seeded fibers were produced as described above, although single fibers intended for both conditions were mounted and pieces sticking out of culture-insert walls were cut out with a scalpel. Finally, the mounted fibers (Figure 4) were transferred to respective polystyrene chambers (Fisher Scientific, Pittsburgh, US) instead of 24-well plates for static and dynamic conditioning.

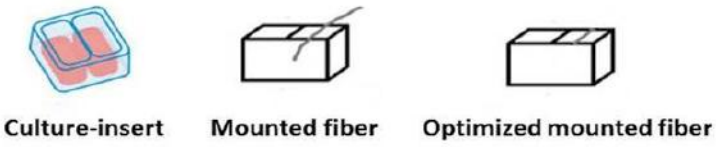

Figure 4 Illustration of a culture-insert (Ibidi) (left) and both ways of mounted fiber pieces on culture-inserts (middle and right).

Foams. Harvested cells were diluted in a cell suspension of 10^6 cells/mL containing respective growth media with 1% HEPES and no FBS. Once the FN protein was thawed at room temperature, it was pipetted on top of pre-coated as well as non-pre-coated with the FN protein cover slips in a 24-well plate. Subsequently, air bubbles were introduced to the protein with a pipette in order to transform the silk solution into a foam construct. Further, the prepared cell suspension was carefully added onto the top of the foam and cell-seeded foams were let to incubate for 30 minutes at 37 °C with 5% CO_2. Once the incubation time was completed, respective medium was carefully added dropwise at the edges around the cell-seeded foam constructs and changed every second day as well.

2.6 Crystal Violet cell adhesion assay

Cell adhesion and morphology on protein-coated well surfaces 24 and 48 hours after cell-seeding was monitored with Crystal Violet assay. In details, cells adhered to the protein-coated wells in a 24-well plate were carefully aspirated growth medium and washed twice with pre-warmed at 37 °C PBS. Subsequently, cells were fixed with 96% ethanol and let to incubate for 10 minutes at room temperature. Once the incubation time was completed, fixed cells were washed thrice with distilled water and stained with 50 µL 0.1% Crystal Violet (Sigma-Aldrich) in deionized water. Further, stained cells were let to incubate for 30 minutes at room temperature under the hood and once the incubation time was completed, they were washed four times with tap water. Stained cells were then let to dry overnight before documenting cell attachment and morphology under the inverted bright field microscope (Nikon Eclipse Ti, Tokyo, Japan).

2.7 Alamar Blue cell viability and growth rate assay

Cell viability and growth rate on protein-coated cover slips as well as cell-seeded foam and fiber matrices were monitored with Alamar Blue (Invitrogen, Paisley, UK) cell viability assay. Alamar Blue assay relies on the incorporation of an oxidation – reduction growth indicator which responds to cells metabolic activity and changes its fluorescence intensity and color. The difference in fluorescence intensity can further be read by a plate reader and provide a general estimation regarding cells number in culture. In details, Alamar Blue was diluted (1:10) in respective growth medium and added to respective wells containing the protein-coated cover slips as well as to foam constructs and mounted on inserts fibers. Diluted Alamar Blue solution was also added to empty wells in order to aid normalizing subsequently acquired fluorescence intensity values. The plates were then let to incubate for two hours at 37 °C and 5% CO_2. Once the incubation time was completed, 100 µL of the incubated solution was transferred to a Griener 96-well plate with a flat bottom (Sigma-Aldrich). The plate was then wrapped in aluminum-foil paper and transferred to the microplate reader (BMG LABTECH, Ortenberg, Germany) in order to measure fluorescence intensity using excitation at 544 nm and emission at 595 nm, according to manufacturer recommendations.

2.8 Cell fixation and cryo-sectioning of cell-seeded 3D matrices

Fibroblasts and endothelial cells onto protein coatings after a culturing period of one and two weeks respectively under both conditions were paraformaldehyde (PFA) fixated. Briefly, respective growth medium was aspirated and cells were washed twice with pre-warmed at 37 °C PBS. Further, cells were fixed with 4% PFA and let to incubate for 10 minutes at room temperature under the hood. PBS was added to the plates which were subsequently sealed with parafilm and stored at 4 °C.

As for the foam and fiber matrices, the exact same fixation process was followed though cell-seeded constructs were preserved in 20% sucrose at 4 °C prior to cryo-sectioning. Cryo-sectioning was performed with the aid of a cryo-stat (Leica CM3050 S, Wetzlar, Germany), kindly granted its use by the department of Anatomy, Physiology and Biochemistry of Swedish University of Agricultural Sciences (Uppsala, Sweden). Briefly, single drops of mounting medium (Tissue-Tek) (Sakura, Torrance, US) were placed on top of fixated samples and let to frozen at -20 °C for 10 minutes approximately. Once the samples frozen, sections of 12.0 mm in thickness each were taken on top of microscope cover glasses (Thermo Fischer Scientific).

2.9 Antibodies staining for protein detection

Fixated cells on protein coatings as well as sectioned samples of 3D matrices were stained with primary antibodies in order to detect important compounds, similarly found on the aortic cusp milieu. More specifically, cells were accordingly stained with primary antibodies for collagen type I (Sigma-Aldrich), collagen type III (Novus Biologicals, Littleton, US), elastin (Abcam, Cambridge, UK), hyaluronic acid (VWR, Radnor, US), and differentiation of fibroblasts into myofibroblasts (Abcam, Cambridge, UK) determination. Briefly, cells were initially permeabilized with 3% Triton-X for 5 minutes and then washed twice with PBS. Further, cells were blocked with 1% goat serum (GS) in PBS for 20 minutes at room temperature and subsequently stained with the respective primary antibodies diluted in 1% GS according to manufacturers recommended dilution factors. Once the incubation time was completed, cells were washed twice with PBS and stained with diluted (1:500) in 1% GS goat AlexaFlour488 (Invitrogen) against respective primary antibody species. Double stainings including in addition diluted (1:40) in 1% GS AlexaFlour594-Phalloidin (Invitrogen) were only used to label cells for collagen type I and elastin detection on protein coatings. DAPI was diluted (1:1000) in PBS and included to stain nuclei. Finally, protein-coated cover slips as well as stained sections were mounted on microscope glasses (Thermo Fischer Scientific) and with cover slides respectively, using in both cases fluorescence mounting medium (Dako).

2.10 Hematoxylin and eosin staining

Cryo-sections were also labeled with hematoxylin and eosin for determining cell distribution and viability into the 3D matrices. Briefly, sections were stained with hematoxylin and let to incubate for 10 minutes at room temperature. Further, they were rinsed under tap water and incubated for 5 minutes with a single drop of water added on top of them. Lastly, sections were stained with eosin for 5 minutes under the hood and washed with tap water once the incubation time was completed. Cover slides were used to firmly seal the microscope glasses with glycerol.

2.11 Quantification analysis of fluorescence images captured on protein coatings

Immunofluorescence images captured on 9 separate areas over each protein-coated cover slip were further analyzed with ImageJ in order to provide comparable information between the two anisotropically conditioned cell types. In details, the captured images were imported on ImageJ and unsharp-masked by 3 (σ value) neighboring pixels and 0.60 adjusted mask weight. The sharpened images were then split respective channels into three (RGB) new ones. The blue channel depicting stained nuclei was used to calculate the number of cells on each image. The green channel containing the detected protein was by default thresholded and converted into a new black (background) and white (information) image. The new image was further inverted to allow better computation of pixel values belonging to detected protein. Black intensity particles (information) were ultimately analyzed in terms of absolute number and total area spanned all over the thresholded image. The quantification analysis involved the computation of the ratio between the total area spanned by black intensity pixel values belonging to detected protein and number of nuclei on each particular image. Ratios were computed for each of the respective nine separate images taken on each cover slip and corresponding mean values were used in plotting. Finally, the increase in percentage of secreted amount of proteins was computed according to the following formula:

$$\frac{|mv_1 - mv_2|}{\frac{(mv_1 + mv_2)}{2}} \cdot 100$$

The mv_1 and mv_2 values represent the mean values of the two conditions in which the cells were exposed to and as calculated from the ratios on the nine separate images captured.

3 Results

3.1 Cell adherence and morphology on protein coatings

In order to investigate whether hDFn and hUVECs could adhere to as well as develop a spread-out morphology to protein-coated surfaces, they were accordingly stained with the Crystal Violet assay. Images captured under the bright field microscope 24 and 48 hours after cell-seeding confirmed the existence of both cell types (Figures 5 and 6) over the WT and FN silk variants. Further, the typical elongated and cobblestone-like morphologies for fibroblasts and endothelial cells respectively were noticed as well. Additionally, an obvious increase in the amount of cells onto the protein-coated wells was also observed between the images taken 24 and 48 hours after seeding process.

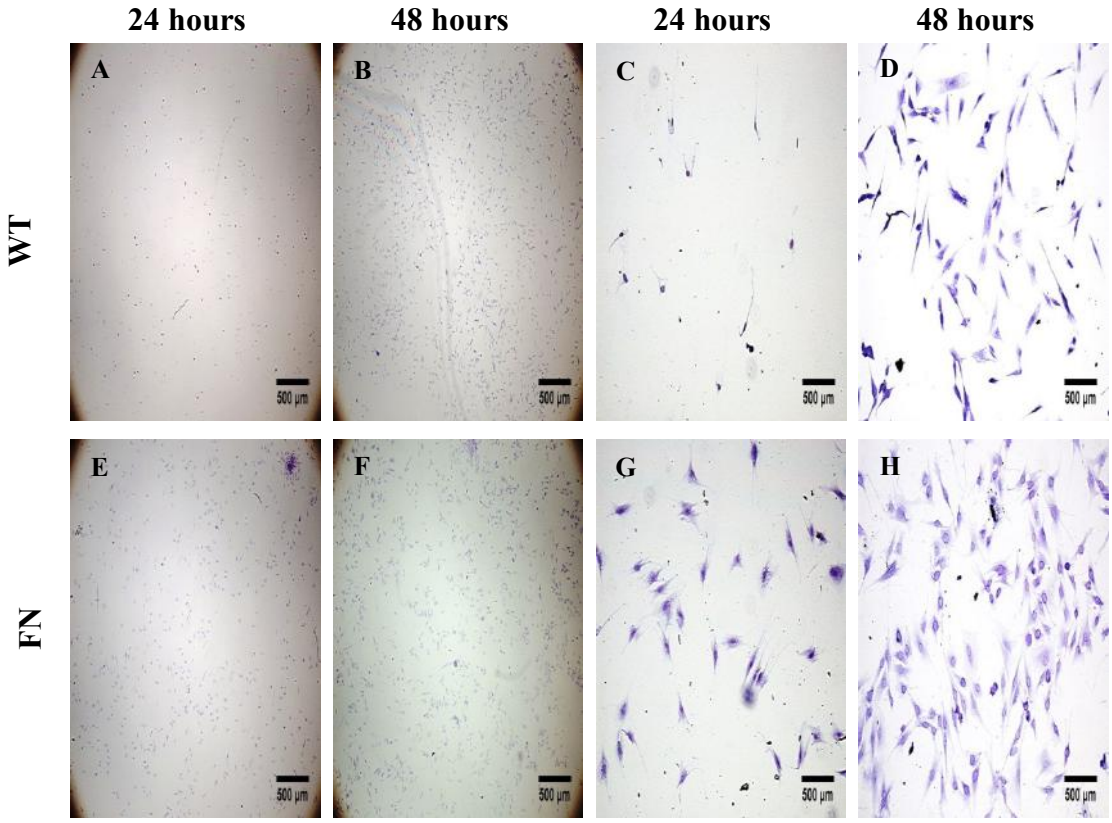

Figure 5 Fibroblasts adhered to the WT and FN protein-coated surfaces in a 24-well plate. Crystal Violet staining of (A) hDFn on WT 24 hours after cell-seeding at 2x magnification, (B) hDFn on WT 48 hours after cell-seeding at 2x magnification, (C) hDFn on WT 24 hours after cell-seeding at 10x magnification, (D) hDFn on WT 48 hours after cell-seeding at 10x magnification, (E) hDFn on FN 24 hours after cell-seeding at 2x magnification, (F) hDFn on FN 48 hours after cell-seeding at 2x magnification, (G) hDFn on FN 24 hours after cell-seeding at 10x magnification, and (H) hDFn on FN 48 hours after cell-seeding at 10x magnification.

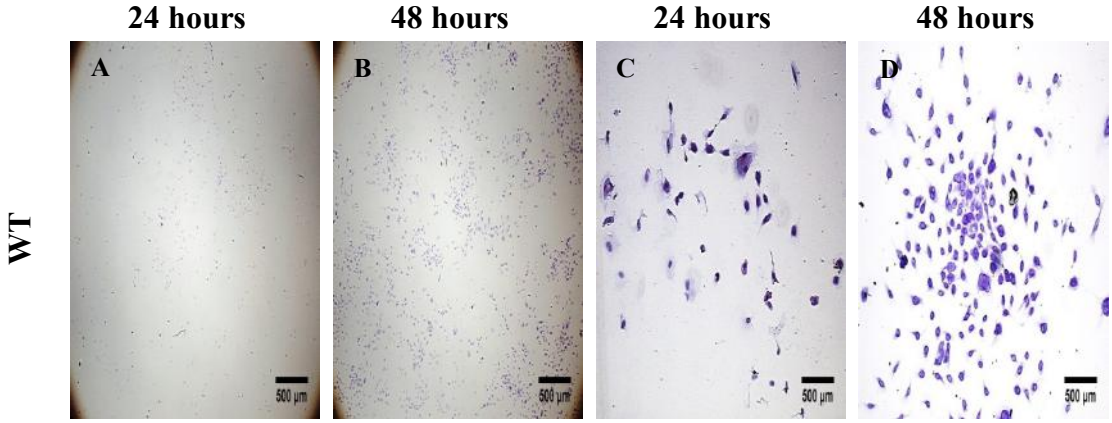

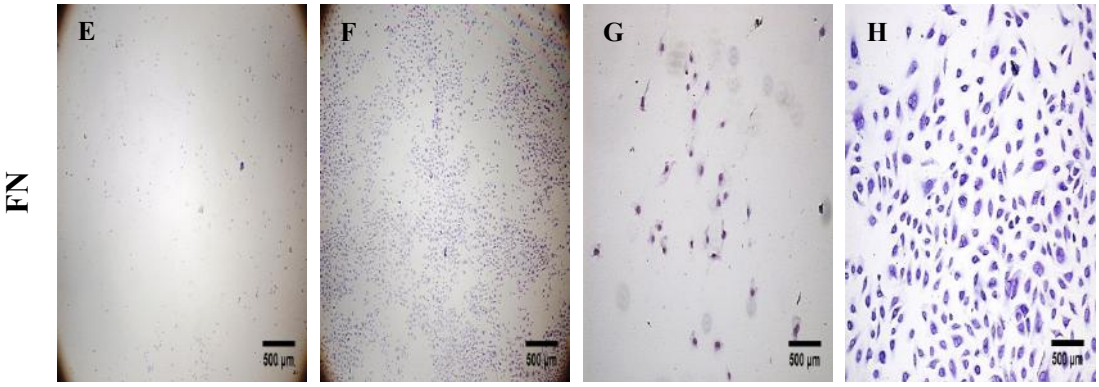

Figure 6 Endothelial cells adhered to the WT and FN protein-coated surfaces in a 24-well plate. Crystal Violet staining of (A) hUVECs on WT 24 hours after cell-seeding at 2x magnification, (B) hUVECs on WT 48 hours after cell-seeding at 2x magnification, (C) hUVECs on WT 24 hours after cell-seeding at 10x magnification, (D) hUVECs on WT 48 hours after cell-seeding at 10x magnification, (E) hUVECs on FN 24 hours after cell-seeding at 2x magnification, (F) hUVECs on FN 48 hours after cell-seeding at 2x magnification, (G) hUVECs on FN 24 hours after cell-seeding at 10x magnification, and (H) hUVECs on FN 48 hours after cell-seeding at 10x magnification.

3.2 Cell viability and growth rate

To investigate cell viability and growth rate onto the protein-coated cover slips as well as into the foam and fiber constructs, both cell types were accordingly introduced to the Alamar Blue assay. Alamar Blue was incorporated to seeded fibroblasts and endothelial cells at pre-defined culture points and prior to changing the speed in the lego-vagga platform.

Protein coatings. Initially, fibroblasts kept in expansion for 8 days were assayed at day 1 and prior to be subjected to the dynamic as well as static conditions. Fluorescence intensity values plotted (Figure 7) indicated a considerable growth rate from starting culture day 1 to final fixation day 8. Fibroblasts were shown to respond to both the vigorous fluid dynamics and under the static conditions, and remarkably proliferate over the WT and FN protein-coated cover slips. Similarly to fibroblasts, fluorescence intensity values on correspondingly assayed with the Alamar Blue endothelial cells were processed and further plotted (Figure 8) as well. In contrast to hDFn, hUVECs were conditioned for 14 days and the rocking platform was switched to higher velocities every fourth culture day. Endothelial cells were introduced to the assay at culture day 2 and finally at culture day 14 prior to cell fixation. Fluorescence intensity values plotted over the two silk variants and control reported profound growth rate under both conditions.

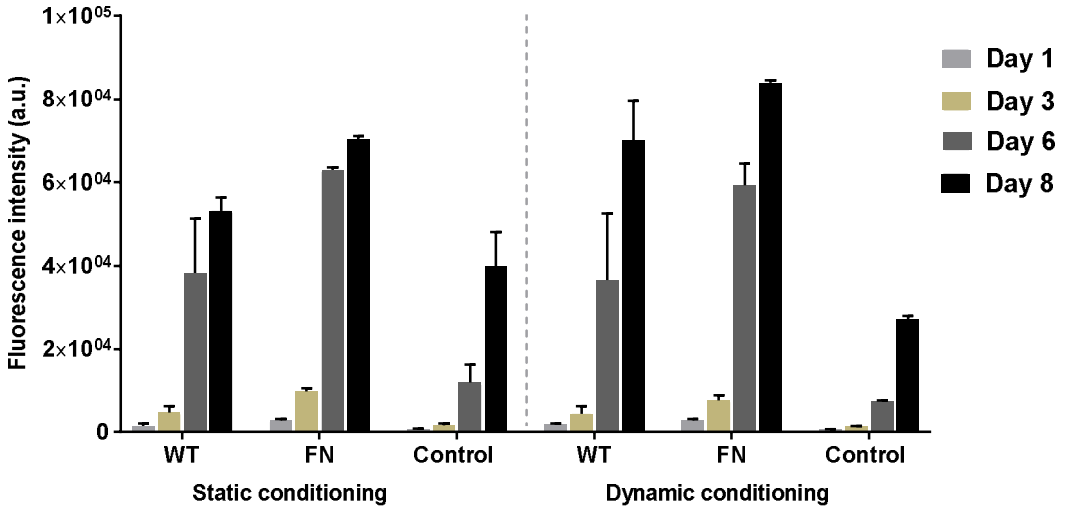

Figure 7 Cell viability and growth rate of hDFn seeded onto the protein-coated cover slips and subjected to both conditions. Fibroblasts were assayed with Alamar Blue and fluorescence intensity values were measured at days 1, 3, 6, and 8 prior to cell fixation. As controls, non-protein pre-coated cover slips seeded with hDFn were used. Normalized mean values $(n = 2, duplicates)$ have been calculated and plotted. Error bars represent maximum values from standard deviation.

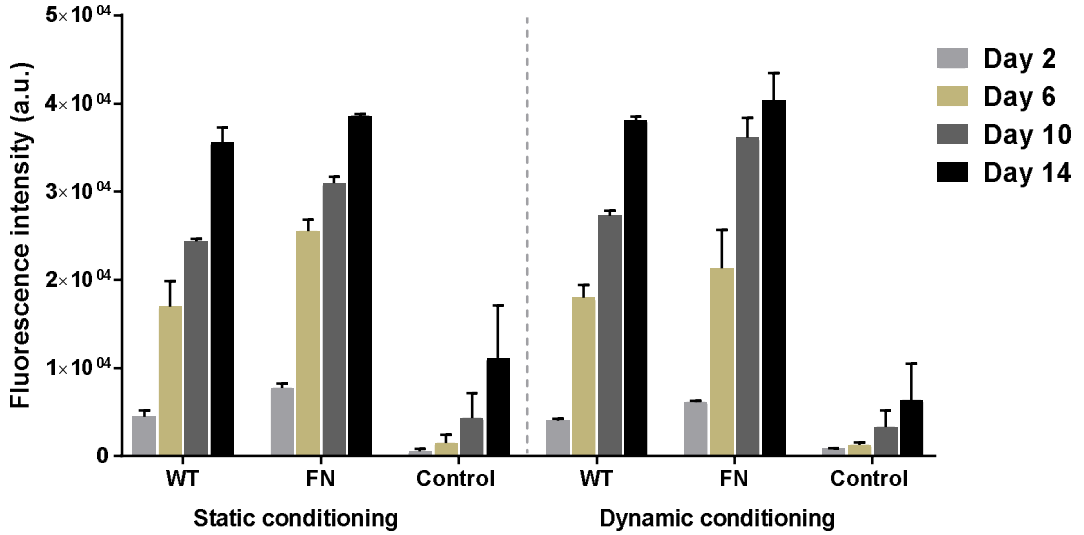

Figure 8 Cell viability and growth rate of hUVECs seeded onto the protein-coated cover slips and subjected to both conditions. Endothelial cells were assayed with Alamar Blue and fluorescence intensity values were measured at days 2, 6, 10, and 14 prior to cell fixation. As controls, non-protein pre-coated cover slips seeded with hUVECs were used. Normalized mean values $(\boldsymbol{n = 2, duplicates})$ have been calculated and plotted. Error bars represent maximum values from standard deviation.

3D matrices. Fibroblasts as well as endothelial cells seeded into the protein-made 3D matrices were also assayed at preset culture time-points, similarly to hUVECs on protein coatings. In particular, all the cell-seeded foam and fiber constructs were initially introduced to the assay at day 2 and prior to be subjected to any of the respective culturing conditions. Fluorescence intensity values processed and further

plotted in relation to culture days indicated a gradual growth for both cell types seeded and dynamically conditioned into the foam pieces (Figures 9 and 10).

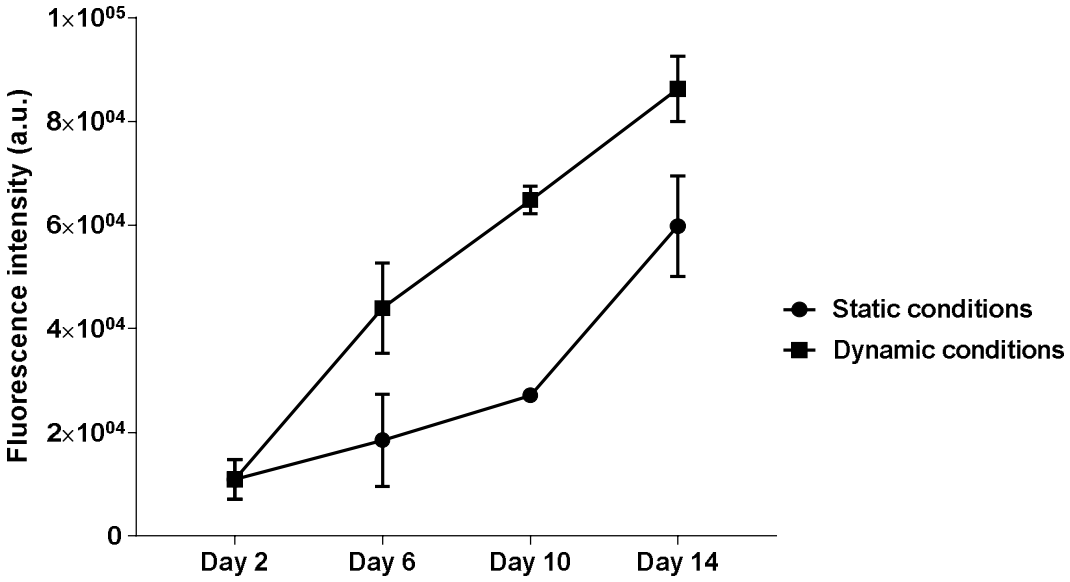

Figure 9 Cell viability and growth rate of hDFn seeded into the protein-made foam constructs and subjected to both conditions. Fibroblasts were assayed with Alamar Blue and fluorescence intensity values were measured at days 2, 6, 10, and 14 prior to cell fixation. Normalized mean values ***(n = 2, duplicates)*** have been calculated and plotted. Mean value at day 2 represents fluorescence intensities obtained by all foam constructs prior to be subjected to any of the two conditions. Error bars represent maximum and minimum values from standard deviation.

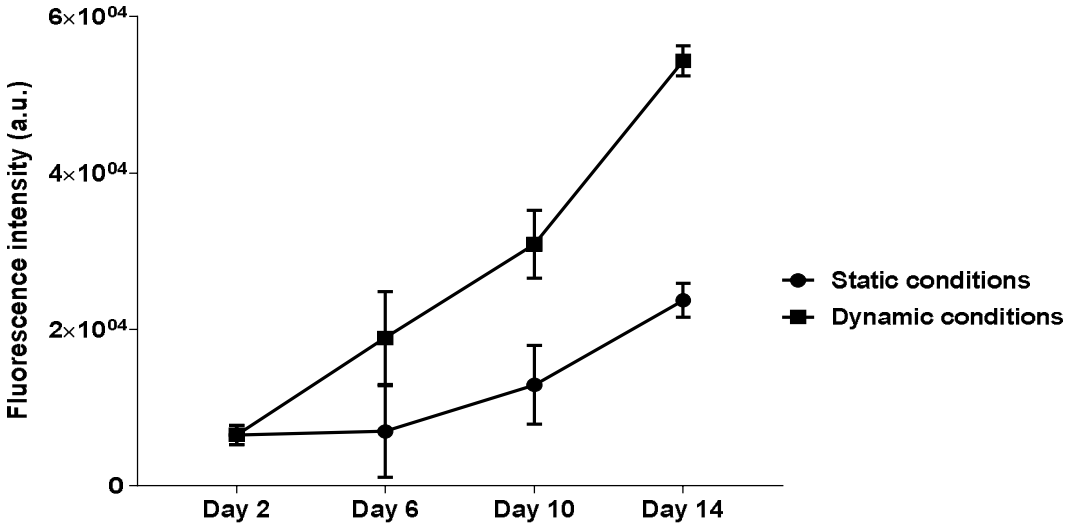

Figure 10 Cell viability and growth rate of hUVECs seeded into the protein-made foam constructs and subjected to both conditions. Endothelial cells were assayed with Alamar Blue and fluorescence intensity values were measured at days 2, 6, 10, and 14 prior to cell fixation. Normalized mean values ***(n = 2, duplicates)*** have been calculated and plotted. Mean value at day 2 represents fluorescence intensities obtained by all foam constructs prior to be subjected to any of the two conditions. Error bars represent maximum and minimum values from standard deviation.

On the contrary, accordingly assayed fibroblasts and endothelial cells into the protein-made fibers were unexpectedly shown (Figures 11 and 12) to proliferate in a higher degree under the static conditions. Fluorescence intensity values measured on statically expanded hDFn displayed a rather rapid cell growth from the initiation of cell culture (day 2) and a subsequent exponentially-like increase (days 10 - 14). Cell growth on dynamically conditioned fibroblasts however illustrated a fairly slow proliferation until day 10, which significantly increases upon applying the highest of fluid dynamics the system could generate.

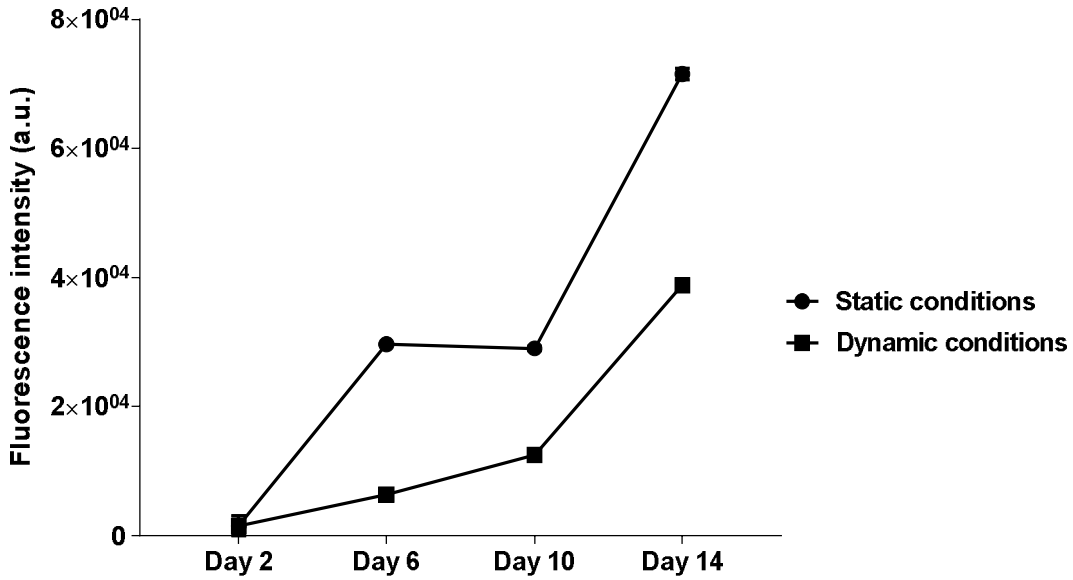

Figure 11 Cell viability and growth rate of hDFn seeded into the protein-made fibers and subjected to both conditions. Fibroblasts were assayed with Alamar Blue and fluorescence intensity values were measured at days 2, 6, 10, and 14 prior to cell fixation. Normalized mean values $(\boldsymbol{n = 2, duplicates})$ have been calculated and plotted. Mean value at day 2 represents fluorescence intensities obtained by all fiber constructs prior to be subjected to any of the two conditions. Error bars (hidden by data point symbols) represent maximum and minimum values from standard deviation.

In contrast to hDFn, the proliferation monitored on the differently conditioned hUVECs appeared to be almost similar until culture day 10. Endothelial cells nevertheless under the static conditions were shown to proliferate faster between culture days 10 and 14, as compared to the respective expanded under shear stresses which retained a more stable growth rate (Figure 12).

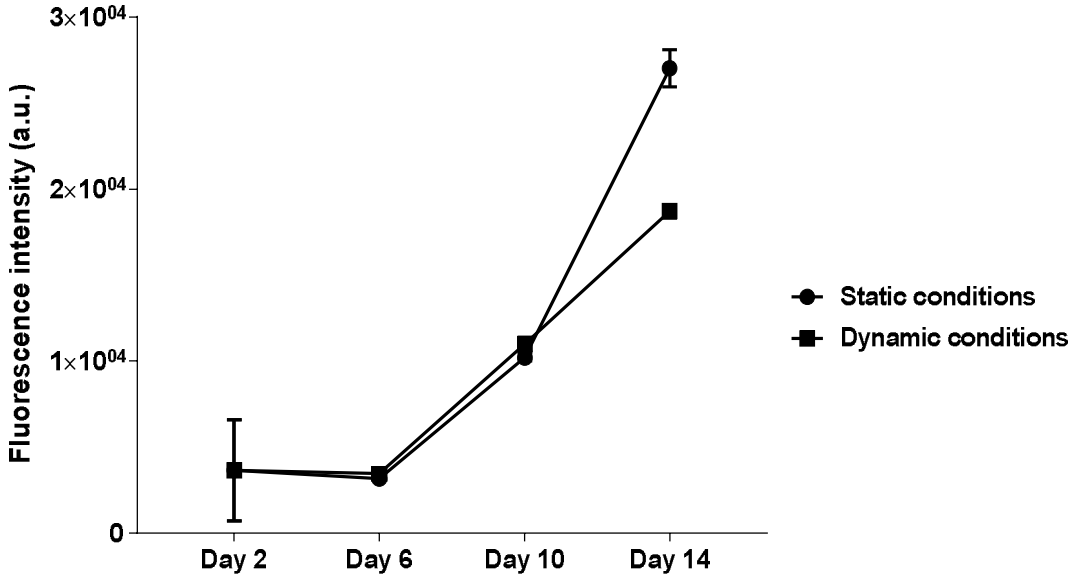

Figure 12 Cell viability and growth rate of hUVECs seeded into the protein-made fibers and subjected to both conditions. Endothelial cells were assayed with Alamar Blue and fluorescence intensity values were measured at days 2, 6, 10, and 14 prior to cell fixation. Normalized mean values ($n = 2, duplicates$) have been calculated and plotted. Mean value at day 2 represents fluorescence intensities obtained by all fiber constructs prior to be subjected to any of the two conditions. Error bars represent maximum and minimum values from standard deviation.

Optimized fiber mounting. At last, cell viability and corresponding growth was also evaluated on the cell-seeded fibers mounted on culture-inserts using the optimized method. In contrast to the previous experimental approach, pieces of cell-seeded fibers intended for each of the respective conditions were known beforehand and mounted individually. Fluorescence intensity values plotted (Figures 13 and 14) demonstrated rather contradictory proliferation patterns between the two anisotropically conditioned cell types. In particular, growth rate in the piece of fiber seeded with hDFn and exposed to shear stresses displayed a gradually increasing profile until the last culture day 14. The respective growth on the fiber cultured under the static conditions though started declining after a very promising initiation phase. On the contrary, the endothelial cell-seeded piece of fiber subjected to fluid dynamics exhibited a fairly low and steady proliferation as compared to the respective piece which was expanded under static conditioning.

Unfortunately, fluorescence intensity values obtained and further processed at culture day 6 were greatly irrelevant to the values found on the rest experimental days. In fact, they were much lower in magnitude as compared to the respective in control wells and thus, they were excluded from subsequent plots due to falsifying information when normalized.

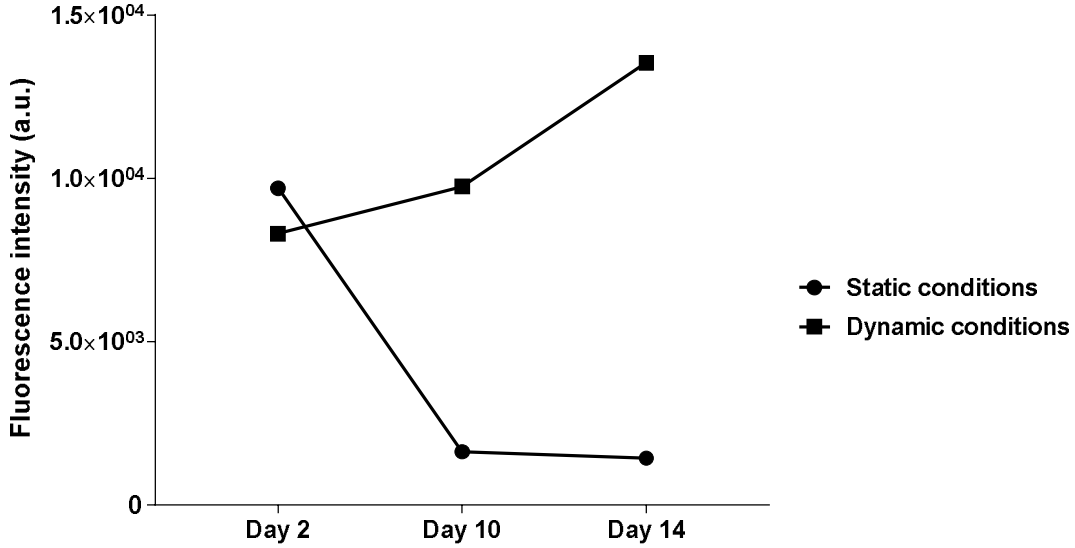

Figure 13 Cell viability and growth rate of hDFn into the protein-made fibers mounted on culture-inserts using the optimized method and exposed to both conditions. Fibroblasts were assayed with Alamar Blue and fluorescence intensity values were measured at days 2, 10, and 14 prior to cell fixation. Normalized mean values ***(n = 2, duplicates)*** have been calculated and plotted. Error bars (hidden by data point symbols) represent maximum and minimum values from standard deviation.

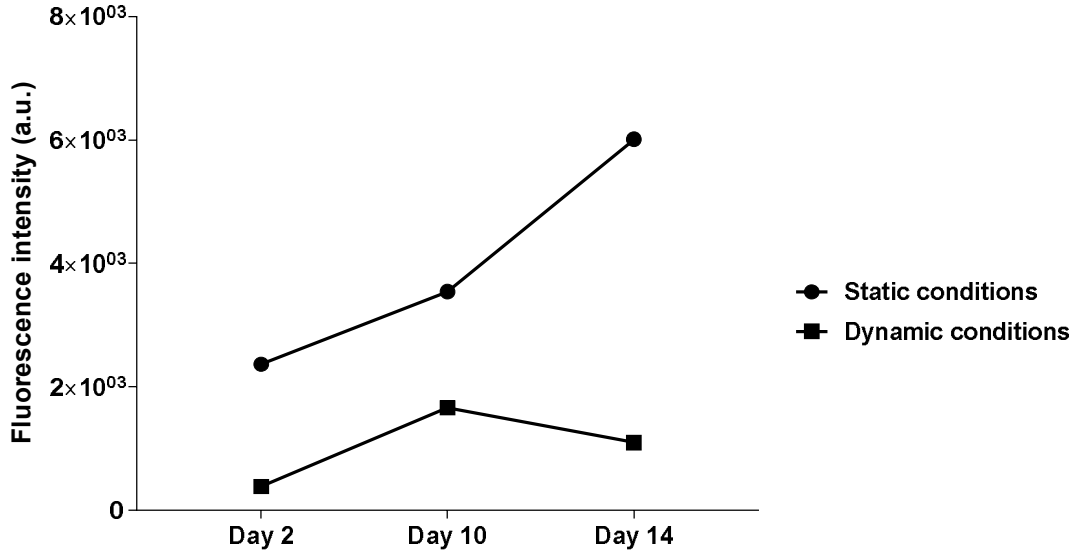

Figure 14 Cell viability and growth rate of hUVECs into the protein-made fibers mounted on culture-inserts using the optimized method and exposed to both conditions. Endothelial cells were assayed with Alamar Blue and fluorescence intensity values were measured at days 2, 10, and 14 prior to cell fixation. Normalized mean values ***(n = 2, duplicates)*** have been calculated and plotted. Error bars (hidden by data point symbols) represent maximum and minimum values from standard deviation.

3.3 Detection of proteins by antibody stainings

Protein coatings. The secretion of tissue-specific proteins by hDFn and hUVECs seeded onto the protein-coated cover slips was determined by staining with respective antibodies. Immunofluorescence images taken on stained fibroblasts displayed a

highly developed fibrous network formation of extracellularly deposited collagen type III (Figure 15). In addition, a noticeable and mainly intracellularly located elastin composition (Figure 16) was detected as well. Findings were similarly observed on both silk variants.

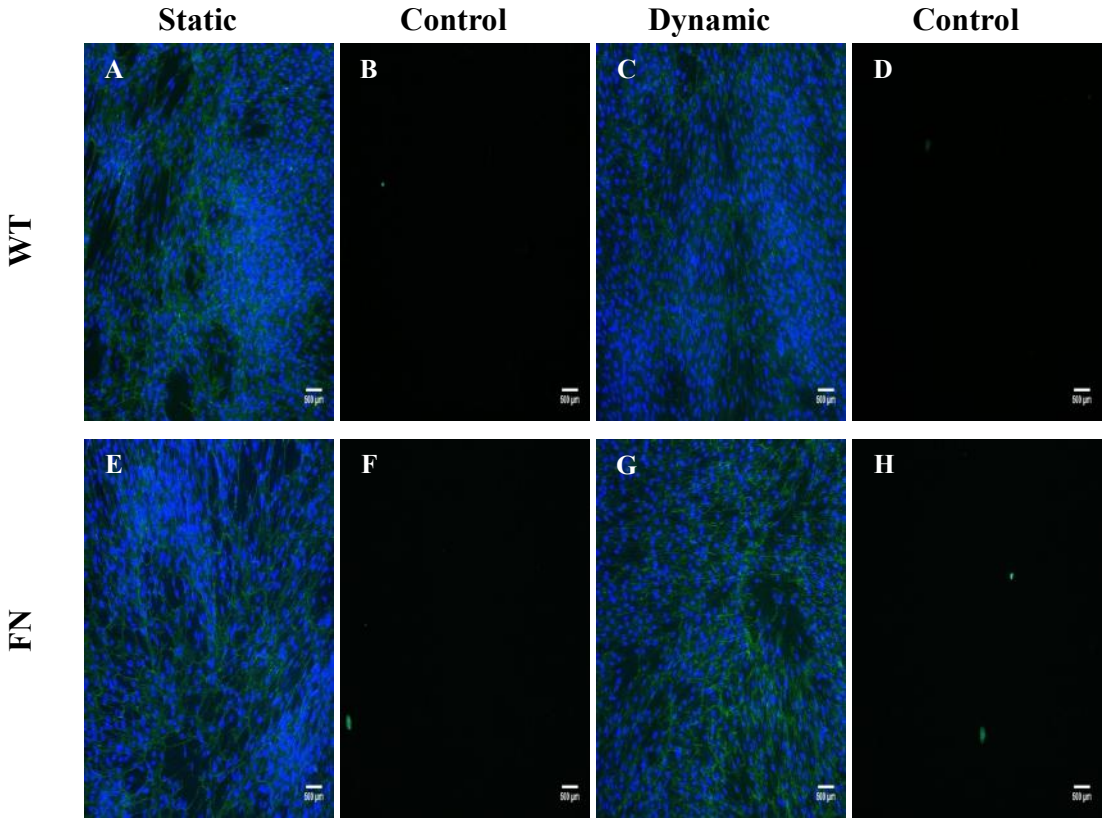

Figure 15 Fibroblasts labeled with the respective antibodies for (A) detection of collagen type III (green) on WT under static conditions at 10x magnification, (B) WT control staining where the primary antibody was excluded (static conditions) at 10x magnification, (C) detection of collagen type III (green) on WT under dynamic conditions at 10x magnification, (D) WT control staining where the primary antibody was excluded (dynamic conditions) at 10x magnification, (E) detection of collagen type III (green) on FN under static conditions at 10x magnification, (F) FN control staining where the primary antibody was excluded (static conditions) at 10x magnification, (G) detection of collagen type III (green) on FN under dynamic conditions at 10x magnification, (H) FN control staining where the primary antibody was excluded (dynamic conditions) at 10x magnification. Nuclei were stained with DAPI (blue) (A, C, E, and G).

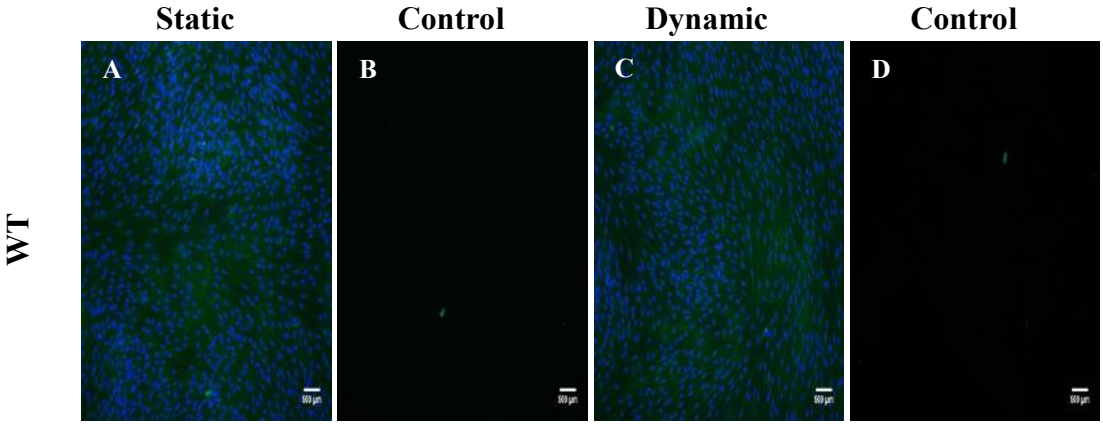

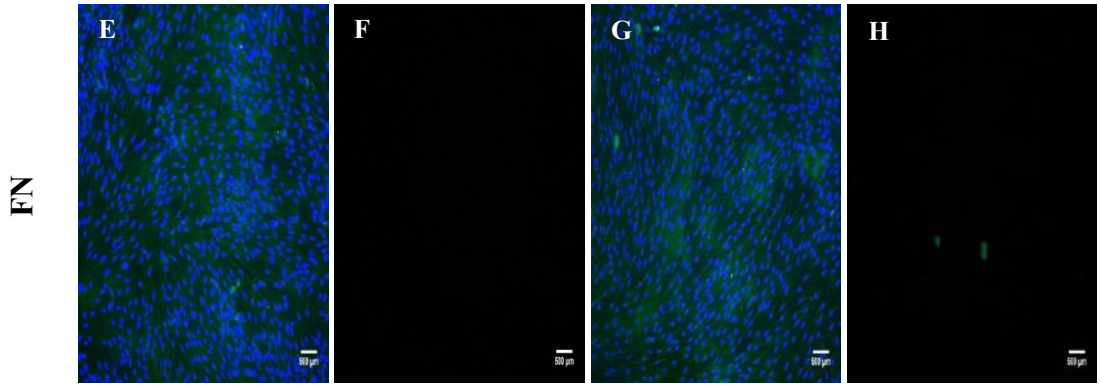

Figure 16 Fibroblasts labeled with the respective antibodies for (A) detection of elastin (green) on WT under static conditions at 10x magnification, (B) WT control staining where the primary antibody was excluded (static conditions) at 10x magnification, (C) detection of elastin (green) on WT under dynamic conditions at 10x magnification, (D) WT control staining where the primary antibody was excluded (dynamic conditions) at 10x magnification, (E) detection of elastin (green) on FN under static conditions at 10x magnification, (F) FN control staining where the primary antibody was excluded (static conditions) at 10x magnification, (G) detection of elastin (green) on FN under dynamic conditions at 10x magnification, (H) FN control staining where the primary antibody was excluded (dynamic conditions) at 10x magnification. Nuclei were stained with DAPI (blue) (A, C, E, and G).

Moreover, fibroblasts accordingly labeled to detect the biological marker αSMA (Figure 17) were positively fluoresced, thereby confirming the differentiation into myofibroblasts on both the protein-coated substrates.

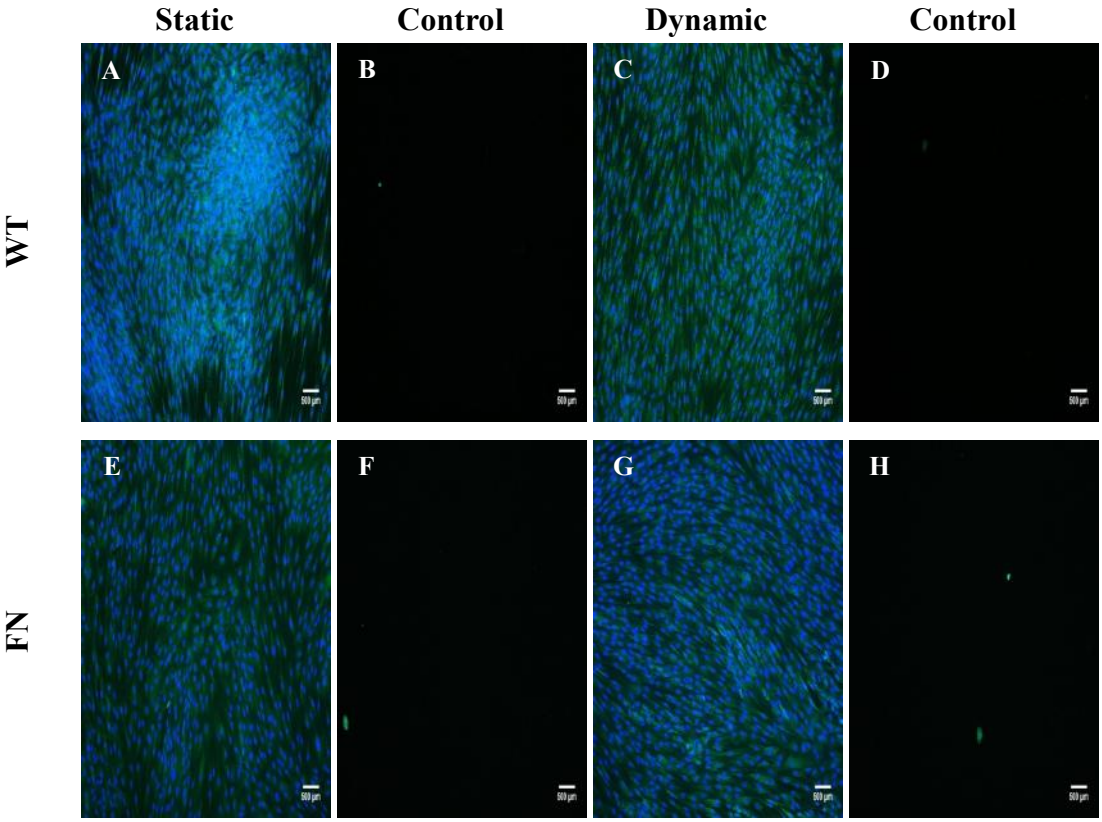

Figure 17 Fibroblasts labeled with the respective antibodies for (A) detection of αSMA (green) on WT under static conditions at 10x magnification, (B) WT control staining where the primary antibody was excluded (static conditions) at 10x magnification, (C) detection of αSMA (green) on WT under dynamic conditions at 10x

magnification, (D) WT control staining where the primary antibody was excluded (dynamic conditions) at 10x magnification, (E) detection of αSMA (green) on FN under static conditions at 10x magnification, (F) FN control staining where the primary antibody was excluded (static conditions) at 10x magnification, (G) detection of αSMA (green) on FN under dynamic conditions at 10x magnification, (H) FN control staining where the primary antibody was excluded (dynamic conditions) at 10x magnification. Nuclei were stained with DAPI (blue) (A, C, E, and G).

The respective antibodies for collagen type I and hyaluronic acid synthesis were also utilized to stain hDFn onto the protein-coated cover slips. However, neither extracellular secretion nor intracellular composition of any of the two proteins could determinately be detected on the immunofluorescence images captured. In fact, the fluorescent signal (green) observed on both silk variants was extremely weak and could not decisively be confirmed on the representative images (Figure 18) taken.

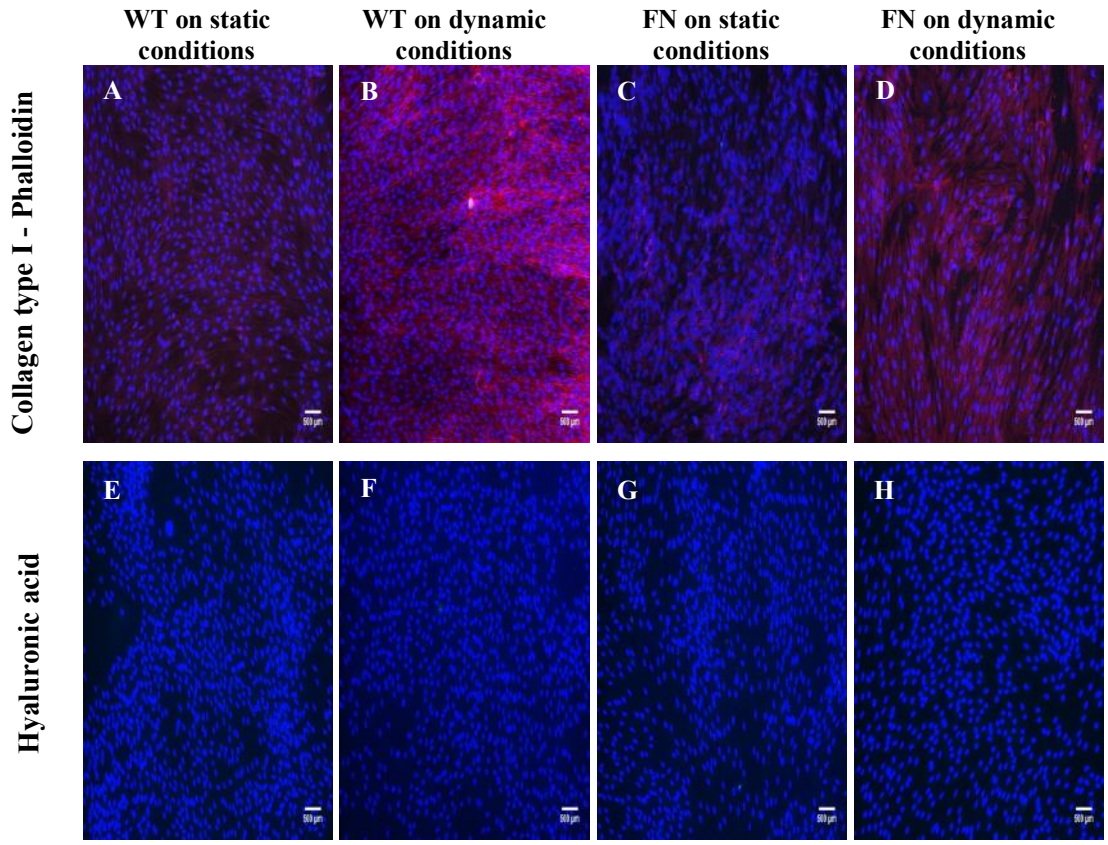

Figure 18 Fibroblasts labeled with the respective antibodies for (A) detection of collagen type I (green) on WT under static conditions at 10x magnification, (B) detection of collagen type I (green) on WT under dynamic conditions at 10x magnification, (C) detection of collagen type I (green) on FN under static conditions at 10x magnification, (D) detection of collagen type I (green) on FN under dynamic conditions at 10x magnification, (E) detection of hyaluronic acid (green) on WT under static conditions at 10x magnification, (F) detection of hyaluronic acid (green) on WT under dynamic conditions at 10x magnification, (G) detection of hyaluronic acid (green) on FN under static conditions at 10x magnification, (H) detection of hyaluronic acid (green) on FN under dynamic conditions at 10x magnification. Fibroblasts were counter-stained with AlexaFlour594-Phalloidin (red) in collagen type I detection. Nuclei were stained with DAPI (blue) (A - H).

Further, hUVECs seeded onto the protein-coated cover slips were also labeled with the respective antibodies. Results on immunofluorescence images captured were

concomitant to a high degree with the corresponding on hDFn findings (Figures 19, 20, and 21). Endothelial cells were also counter-stained with AlexaFlour594-Phalloidin to determine whether the elastin was extracellularly secreted or intracellularly composed.

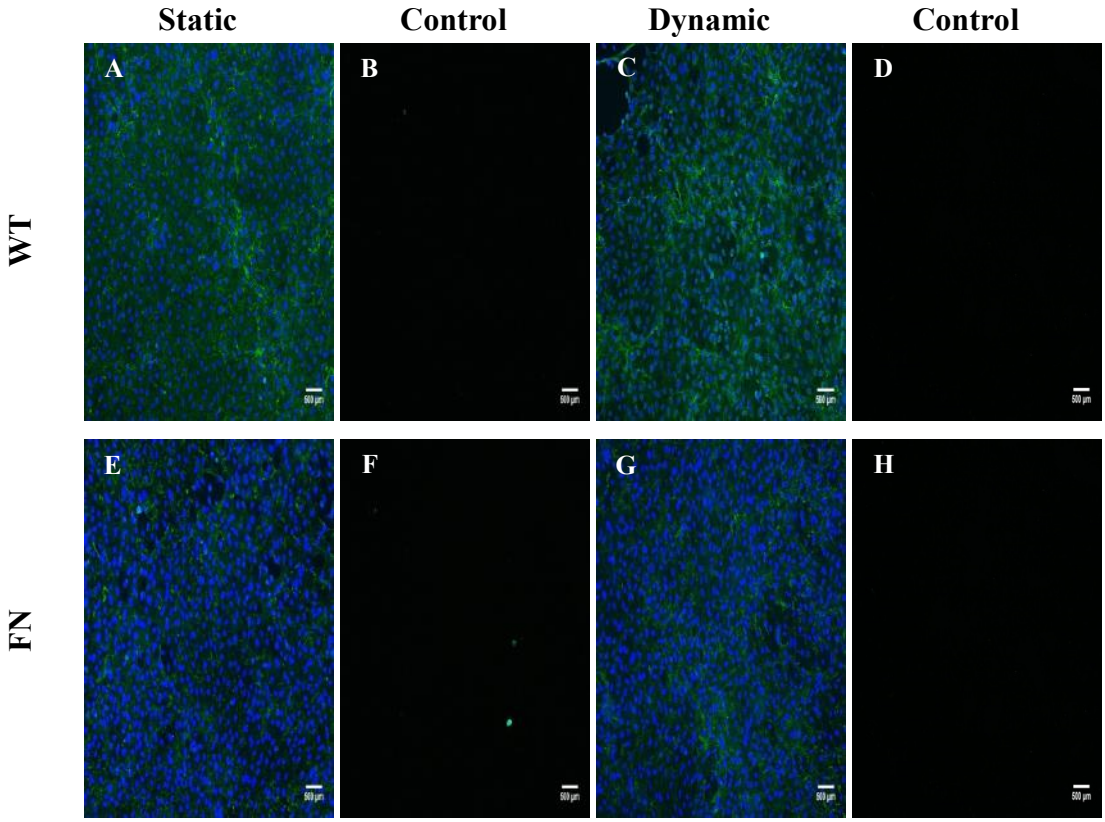

Figure 19 Endothelial cells labeled with the respective antibodies for (A) detection of collagen type III (green) on WT under static conditions at 10x magnification, (B) WT control staining where the primary antibody was excluded (static conditions) at 10x magnification, (C) detection of collagen type III (green) on WT under dynamic conditions at 10x magnification, (D) WT control staining where the primary antibody was excluded (dynamic conditions) at 10x magnification, (E) detection of collagen type III (green) on FN under static conditions at 10x magnification, (F) FN control staining where the primary antibody was excluded (static conditions) at 10x magnification, (G) detection of collagen type III (green) on FN under dynamic conditions at 10x magnification, (H) FN control staining where the primary antibody was excluded (dynamic conditions) at 10x magnification. Nuclei were stained with DAPI (blue) (A, C, E, and G).

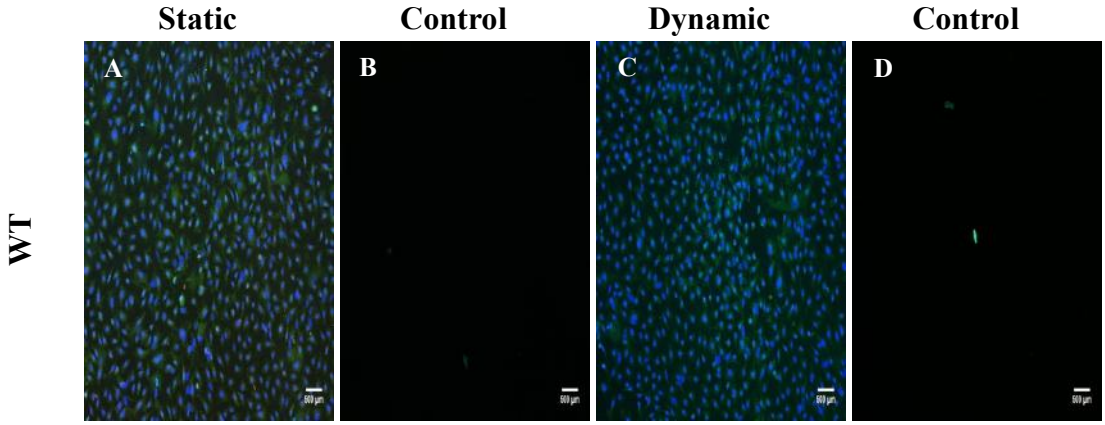

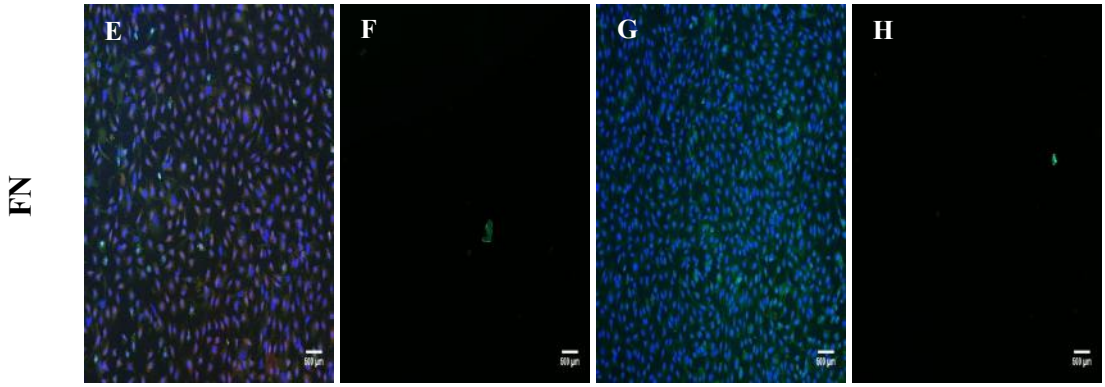

Figure 20 Endothelial cells labeled with the respective antibodies for (A) detection of elastin (green) on WT under static conditions at 10x magnification, (B) WT control staining where the primary antibody was excluded (static conditions) at 10x magnification, (C) detection of elastin (green) on WT under dynamic conditions at 10x magnification, (D) WT control staining where the primary antibody was excluded (dynamic conditions) at 10x magnification, (E) detection of elastin (green) on FN under static conditions at 10x magnification, (F) FN control staining where the primary antibody was excluded (static conditions) at 10x magnification, (G) detection of elastin (green) on FN under dynamic conditions at 10x magnification, (H) FN control staining where the primary antibody was excluded (dynamic conditions) at 10x magnification. Nuclei were stained with DAPI (blue) (A, C, E, and G).

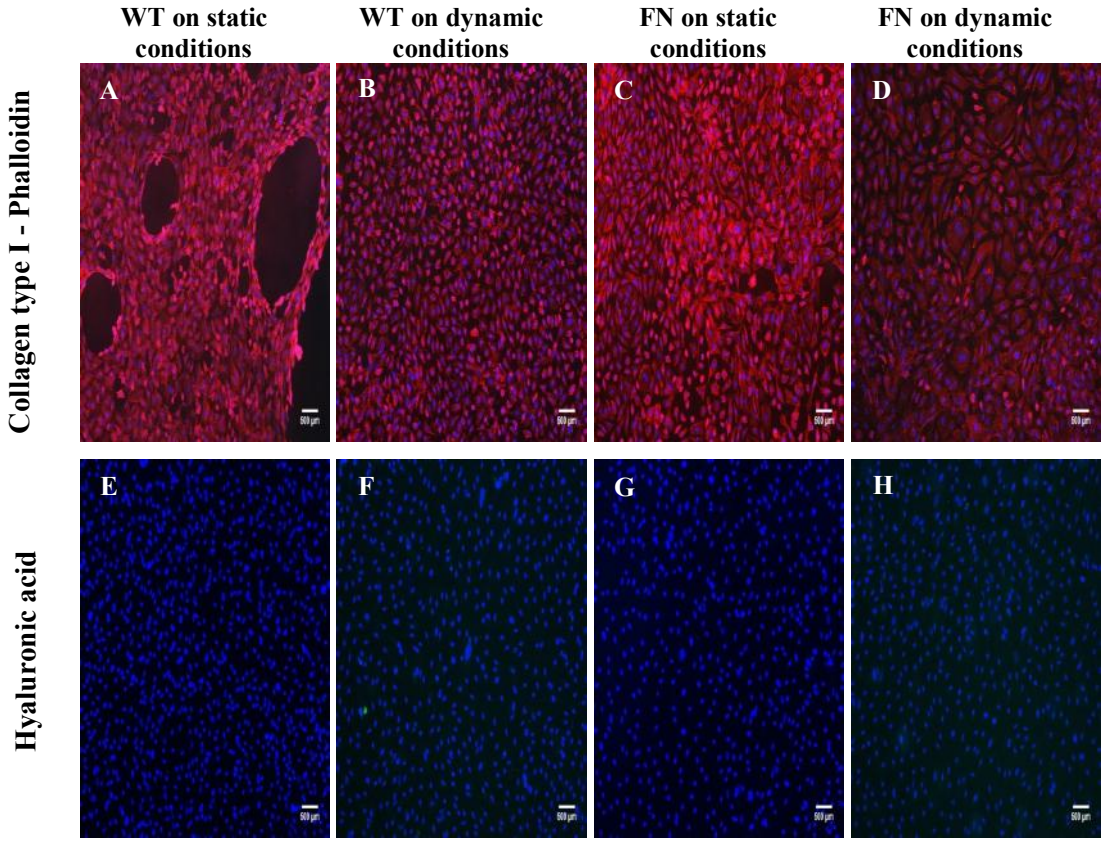

Figure 21 Endothelial cells labeled with the respective antibodies for (A) detection of collagen type I (green) on WT under static conditions at 10x magnification, (B) detection of collagen type I (green) on WT under dynamic conditions at 10x magnification, (C) detection of collagen type I (green) on FN under static conditions at 10x magnification, (D) detection of collagen type I (green) on FN under dynamic conditions at 10x magnification, (E) detection of hyaluronic acid (green) on WT under static conditions at 10x magnification, (F) detection of hyaluronic acid (green) on WT under dynamic conditions at 10x magnification, (G) detection of hyaluronic acid (green) on FN under static conditions at 10x magnification, (H) detection of hyaluronic acid (green) on FN under

dynamic conditions at 10x magnification. Endothelial cells were counter-stained with AlexaFlour594-Phalloidin (red) in collagen type I detection. Nuclei were stained with DAPI (blue) (A - H).

Conclusively, immunofluorescence images captured under the microscope indicated a large amount of secreted collagen type III and synthesized elastin by both cell types seeded. In addition, the differentiation of fibroblasts into myofibroblasts was also confirmed by the positively fluoresced cells in αSMA detection. Collagen type I as well as hyaluronic acid was nevertheless weakly detected on both the anisotropically conditioned substrates seeded with hDFn and hUVECs.

3D matrices. Similarly to protein coatings, antibody stainings were also utilized to label cells into the protein-made scaffolds in order to detect the secreted compounds.

Foam scaffolds. Immunofluorescence images captured on stained fibroblasts into the foam constructs (Figure 22) identified the existence of collagen type I and elastin and in addition, confirmed the detection of hyaluronic acid on the dynamically conditioned cells. Collagen type III as well as the αSMA marker is nevertheless difficult to be demonstrated, as accordingly stained sections are greatly alike to respective controls. In contrast to cells exposed to fluid dynamics, hyaluronic acid was not produced by the statically conditioned fibroblasts.

On the contrary, collagen type I was not detected on either the statically or dynamically conditioned hUVECs into the foam scaffolds (Figure 23). Collagen type III as well as hyaluronic acid was found to have been produced only by the endothelial cells expanded under the shear stresses. Elastin nevertheless was remarkably synthesized in large amounts into the foam matrices that were exposed to both conditions.

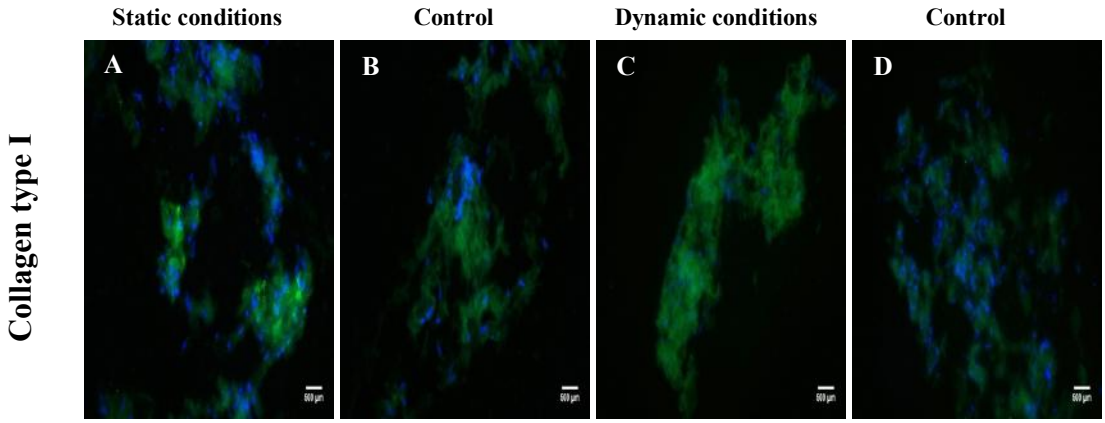

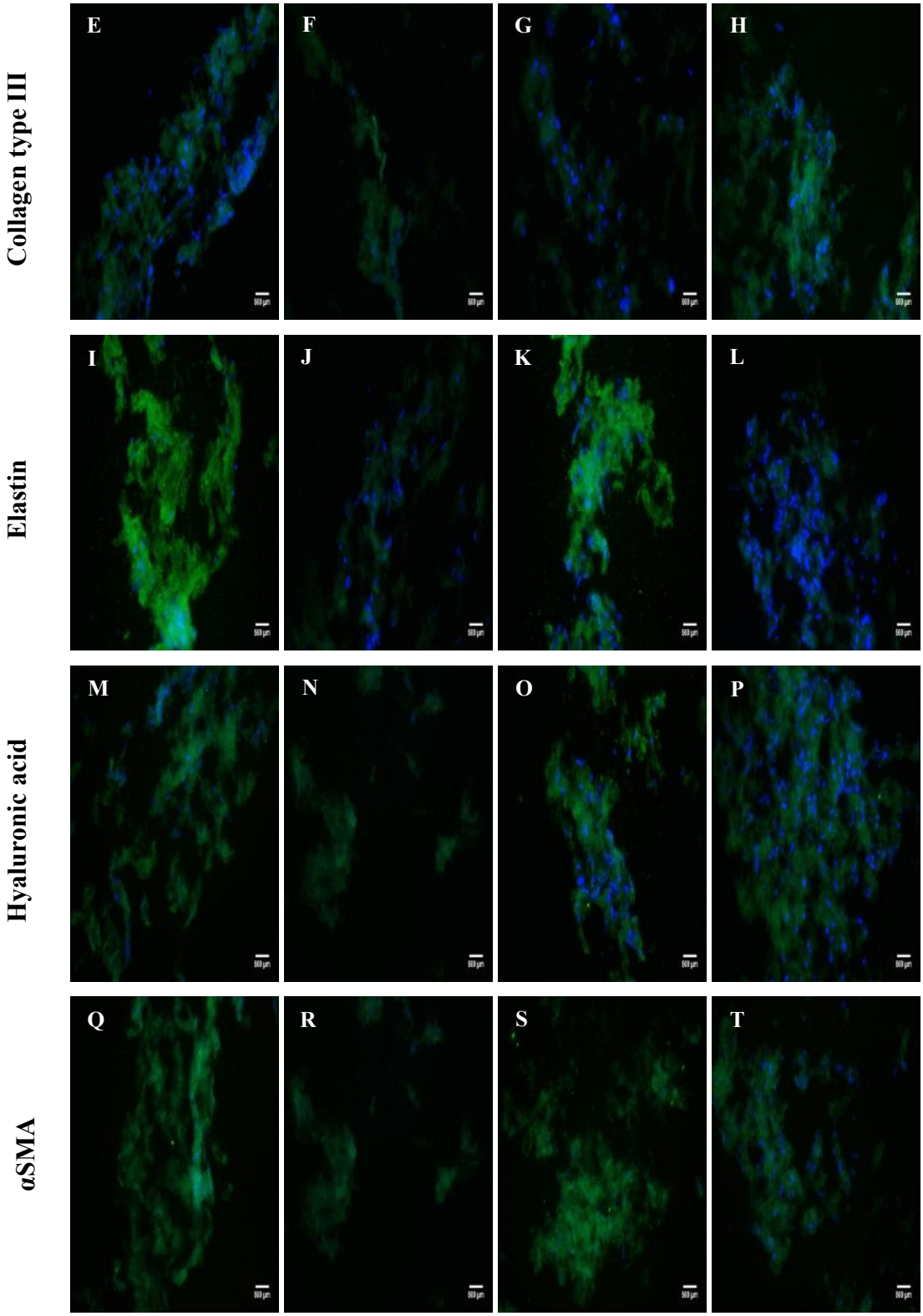

Figure 22 Fibroblasts seeded into foam constructs sectioned and accordingly stained for (A) collagen type I detection under static conditions at 20x magnification, (B) mouse control detection where the primary antibody was excluded (static conditions) at 20x magnification, (C) collagen type I detection under dynamic conditions at 20x magnification, (D) mouse control detection where the primary antibody was excluded (dynamic conditions) at 20x magnification, (E) collagen type III detection under static conditions at 20x magnification, (F) rabbit control detection where the primary antibody was excluded (static conditions) at 20x magnification, (G) collagen type III detection under dynamic conditions at 20x magnification, (H) rabbit control detection where the primary antibody

was excluded (dynamic conditions) at 20x magnification, (I) elastin detection under static conditions at 20x magnification, (J) guinea pig control detection where the primary antibody was excluded (static conditions) at 20x magnification, (K) elastin detection under dynamic conditions at 20x magnification, (L) guinea pig control detection where the primary antibody was excluded (dynamic conditions) at 20x magnification, (M) hyaluronic acid detection under static conditions at 20x magnification, (N) rabbit control detection where the primary antibody was excluded (static conditions) at 20x magnification, (O) hyaluronic acid detection under dynamic conditions at 20x magnification, (P) rabbit control detection where the primary antibody was excluded (dynamic conditions) at 20x magnification, (Q) αSMA detection under static conditions at 20x magnification, (R) rabbit control detection where the primary antibody was excluded (static conditions) at 20x magnification, (S) αSMA detection under dynamic conditions at 20x magnification, and (T) rabbit control detection where the primary antibody was excluded (dynamic conditions) at 20x magnification. Nuclei were stained with DAPI (blue) (A – T).

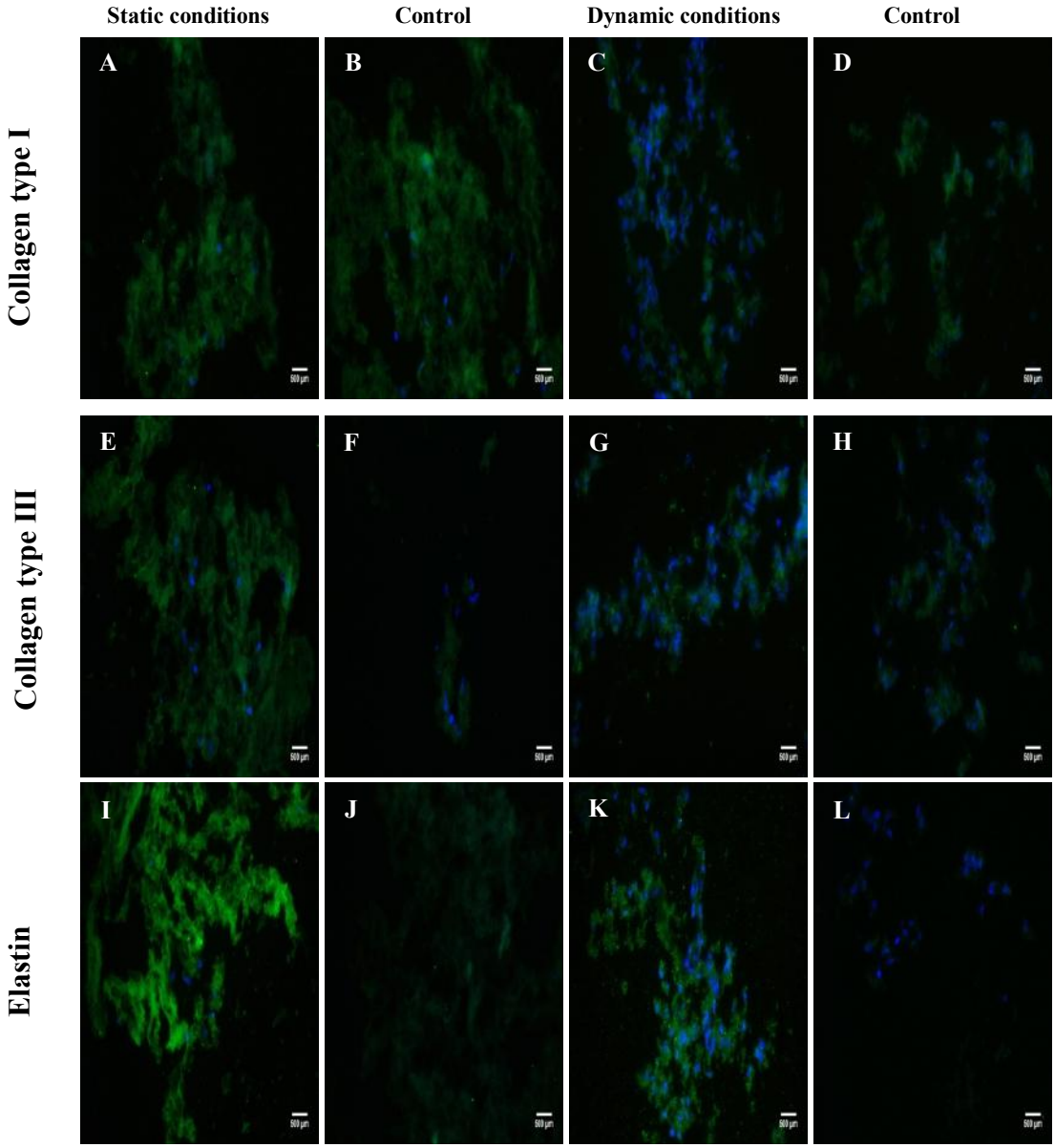

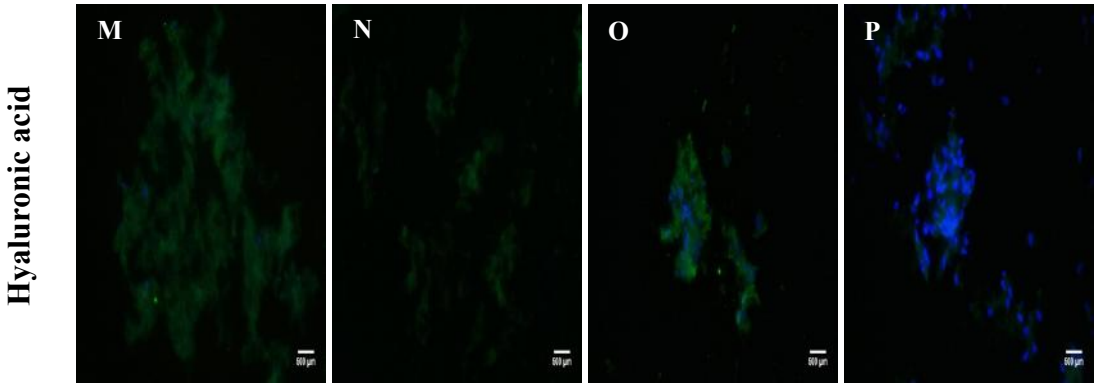

Figure 23 Endothelial cells seeded into foam constructs sectioned and accordingly stained for (A) collagen type I detection under static conditions at 20x magnification, (B) mouse control detection where the primary antibody was excluded (static conditions) at 20x magnification, (C) collagen type I detection under dynamic conditions at 20x magnification, (D) mouse control detection where the primary antibody was excluded (dynamic conditions) at 20x magnification, (E) collagen type III detection under static conditions at 20x magnification, (F) rabbit control detection where the primary antibody was excluded (static conditions) at 20x magnification, (G) collagen type III detection under dynamic conditions at 20x magnification, (H) rabbit control detection where the primary antibody was excluded (dynamic conditions) at 20x magnification, (I) elastin detection under static conditions at 20x magnification, (J) guinea pig control detection where the primary antibody was excluded (static conditions) at 20x magnification, (K) elastin detection under dynamic conditions at 20x magnification, (L) guinea pig control detection where the primary antibody was excluded (dynamic conditions) at 20x magnification, (M) hyaluronic acid detection under static conditions at 20x magnification, (N) rabbit control detection where the primary antibody was excluded (static conditions) at 20x magnification, (O) hyaluronic acid detection under dynamic conditions at 20x magnification, (P) rabbit control detection where the primary antibody was excluded (dynamic conditions) at 20x magnification. Nuclei were stained with DAPI (blue) (A – P).

Fiber scaffolds. Accordingly stained fibroblasts into the protein-made fibers (Figure 24) on the other hand were found poorly secretory in collagen type I. Significant amount of the protein was not detected in any of the two distinct culturing conditions hDFn were subjected to. Collagen type III and hyaluronic acid synthesis as well as αSMA detection is also rather difficult to be confirmed. However, fibroblasts under the shear stresses were seemingly found to have produced hyaluronic acid. Elastin though has been identified in relatively large amounts on both the statically and dynamically conditioned fibroblasts into the fiber pieces.

On the contrary, endothelial cells into the fiber constructs (Figure 25) cultured under the shear stresses have been positively fluoresced in collagen type III and hyaluronic acid detection. Hyaluronic acid was also observed on the images captured on the statically conditioned hUVECs. Elastin deposition was noticeably found in sufficient amounts on both the anisotropically conditioned fiber matrices. Similarly to hUVECs into foam scaffolds, endothelial cells were not found secretory in collagen type I as well.

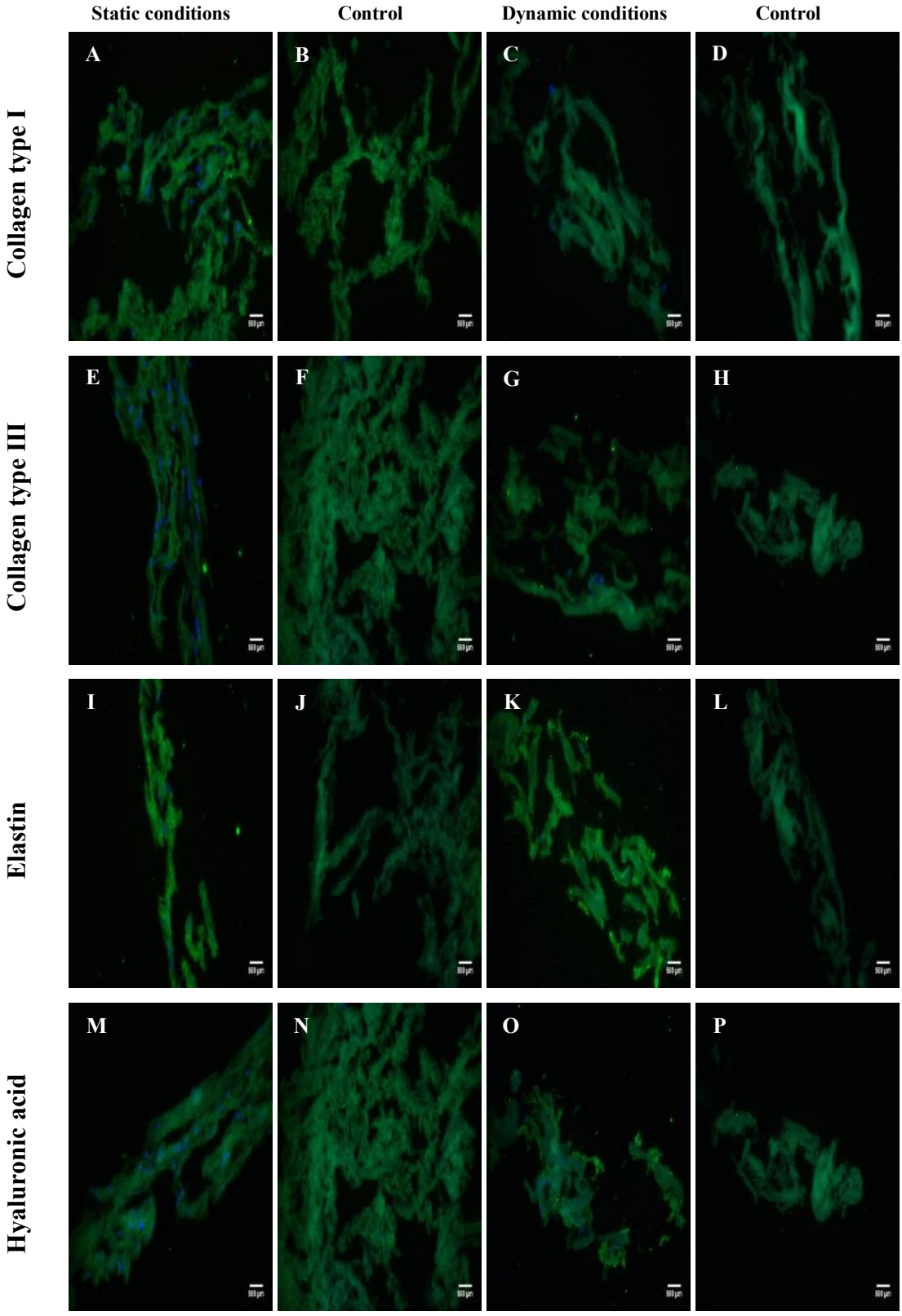
Static conditions
Control
Dynamic conditions
Control
Collagen type I
Collagen type III
Elastin
Hyaluronic acid
A
B
C
D
E
F
G
H
I
J
K
L
M
N
O
P

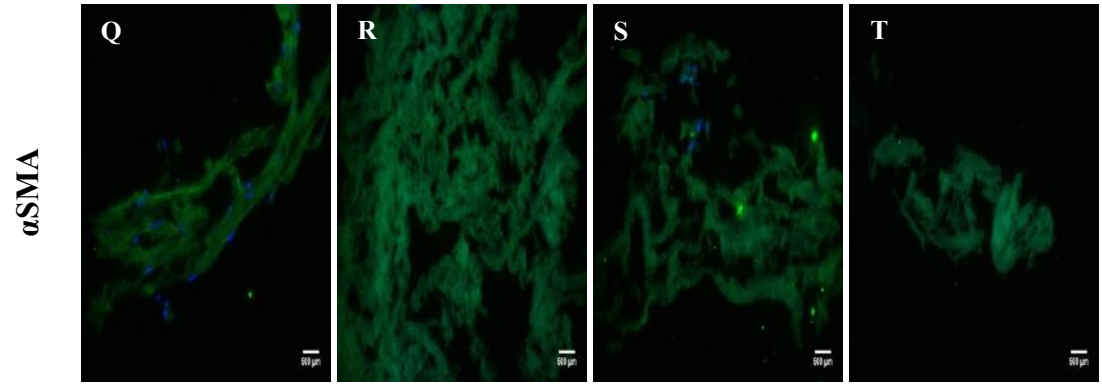

Figure 24 Fibroblasts seeded into fiber constructs sectioned and accordingly stained for (A) collagen type I detection under static conditions at 20x magnification, (B) mouse control detection where the primary antibody was excluded (static conditions) at 20x magnification, (C) collagen type I detection under dynamic conditions at 20x magnification, (D) mouse control detection where the primary antibody was excluded (dynamic conditions) at 20x magnification, (E) collagen type III detection under static conditions at 20x magnification, (F) rabbit control detection where the primary antibody was excluded (static conditions) at 20x magnification, (G) collagen type III detection under dynamic conditions at 20x magnification, (H) rabbit control detection where the primary antibody was excluded (dynamic conditions) at 20x magnification, (I) elastin detection under static conditions at 20x magnification, (J) guinea pig control detection where the primary antibody was excluded (static conditions) at 20x magnification, (K) elastin detection under dynamic conditions at 20x magnification, (L) guinea pig control detection where the primary antibody was excluded (dynamic conditions) at 20x magnification, (M) hyaluronic acid detection under static conditions at 20x magnification, (N) rabbit control detection where the primary antibody was excluded (static conditions) at 20x magnification, (O) hyaluronic acid detection under dynamic conditions at 20x magnification, (P) rabbit control detection where the primary antibody was excluded (dynamic conditions) at 20x magnification, (Q) αSMA detection under static conditions at 20x magnification, (R) rabbit control detection where the primary antibody was excluded (static conditions) at 20x magnification, (S) αSMA detection under dynamic conditions at 20x magnification, and (T) rabbit control detection where the primary antibody was excluded (dynamic conditions) at 20x magnification. Nuclei were stained with DAPI (blue) (A – T).

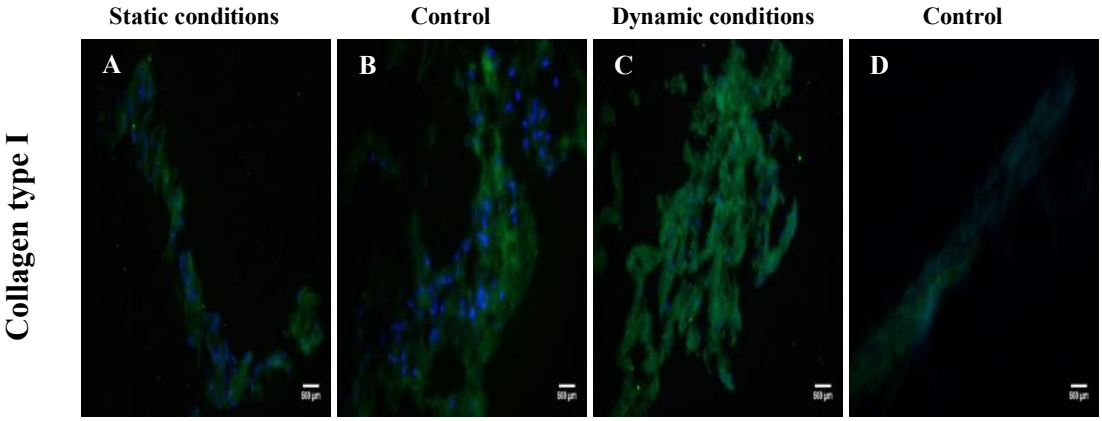

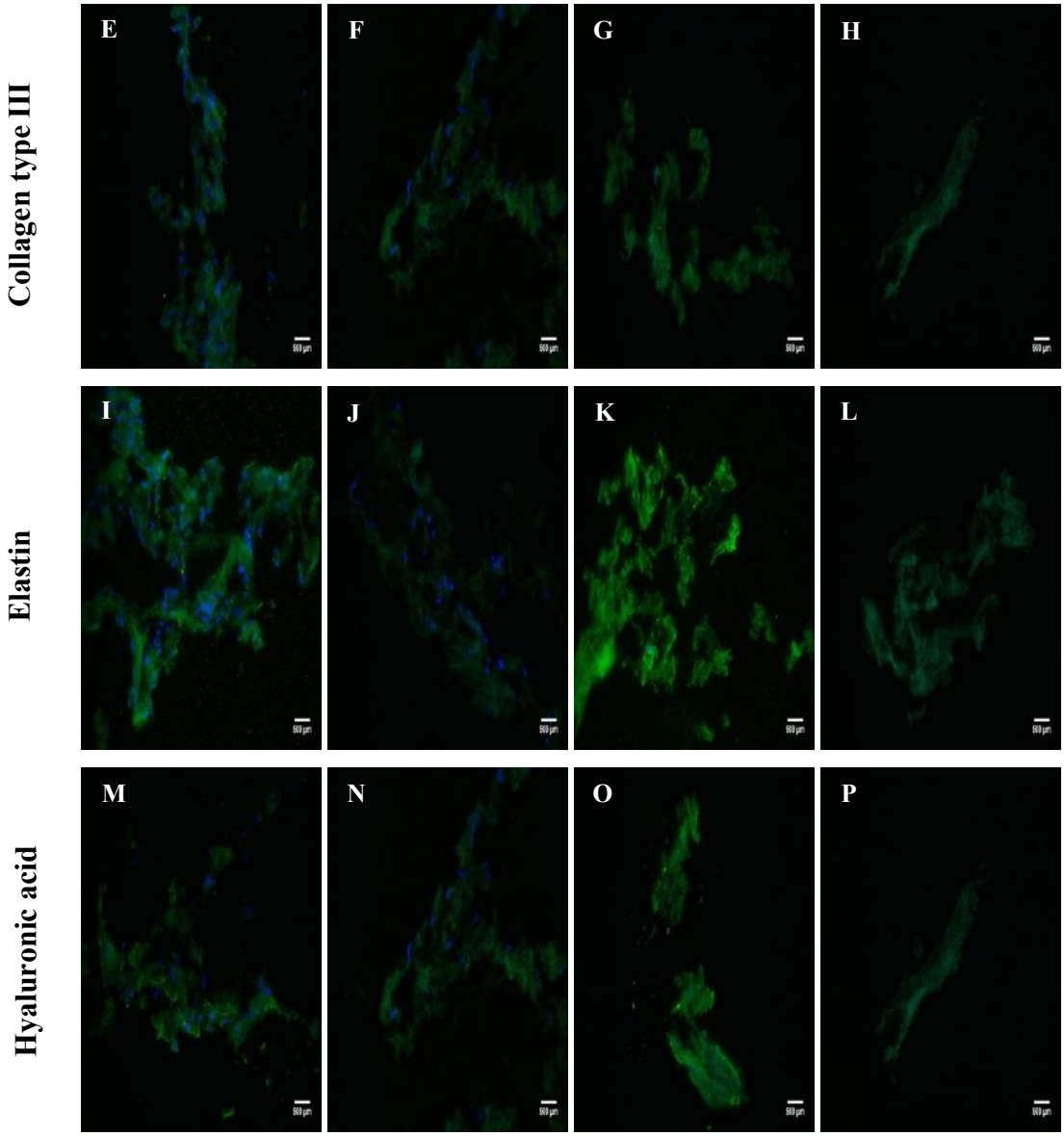

Figure 25 Endothelial cells seeded into fiber constructs sectioned and accordingly stained for (A) collagen type I detection under static conditions at 20x magnification, (B) mouse control detection where the primary antibody was excluded (static conditions) at 20x magnification, (C) collagen type I detection under dynamic conditions at 20x magnification, (D) mouse control detection where the primary antibody was excluded (dynamic conditions) at 20x magnification, (E) collagen type III detection under static conditions at 20x magnification, (F) rabbit control detection where the primary antibody was excluded (static conditions) at 20x magnification, (G) collagen type III detection under dynamic conditions at 20x magnification, (H) rabbit control detection where the primary antibody was excluded (dynamic conditions) at 20x magnification, (I) elastin detection under static conditions at 20x magnification, (J) guinea pig control detection where the primary antibody was excluded (static conditions) at 20x magnification, (K) elastin detection under dynamic conditions at 20x magnification, (L) guinea pig control detection where the primary antibody was excluded (dynamic conditions) at 20x magnification, (M) hyaluronic acid detection under static conditions at 20x magnification, (N) rabbit control detection where the primary antibody was excluded (static conditions) at 20x magnification, (O) hyaluronic acid detection under dynamic conditions at 20x magnification, (P) rabbit control detection where the primary antibody was excluded (dynamic conditions) at 20x magnification. Nuclei were stained with DAPI (blue) (A – P).

Optimized fiber mounting. Similarly to the non-optimized approach, fibroblasts as well as endothelial cells were accordingly stained for determining protein synthesis

(Figures 26 and 27). Collagen type I and III, elastin, and hyaluronic acid production was confirmed by stained hDFn into the fiber pieces mounted using the optimized method. The differentiation into myofibroblasts by detecting the αSMA marker was nevertheless hard to be specified as stained sections were alike controls. Endothelial cells on the other hand were not detectable in collagen type I secretion, but they do have synthesized collagen type III, elastin, and hyaluronic acid under both conditions.

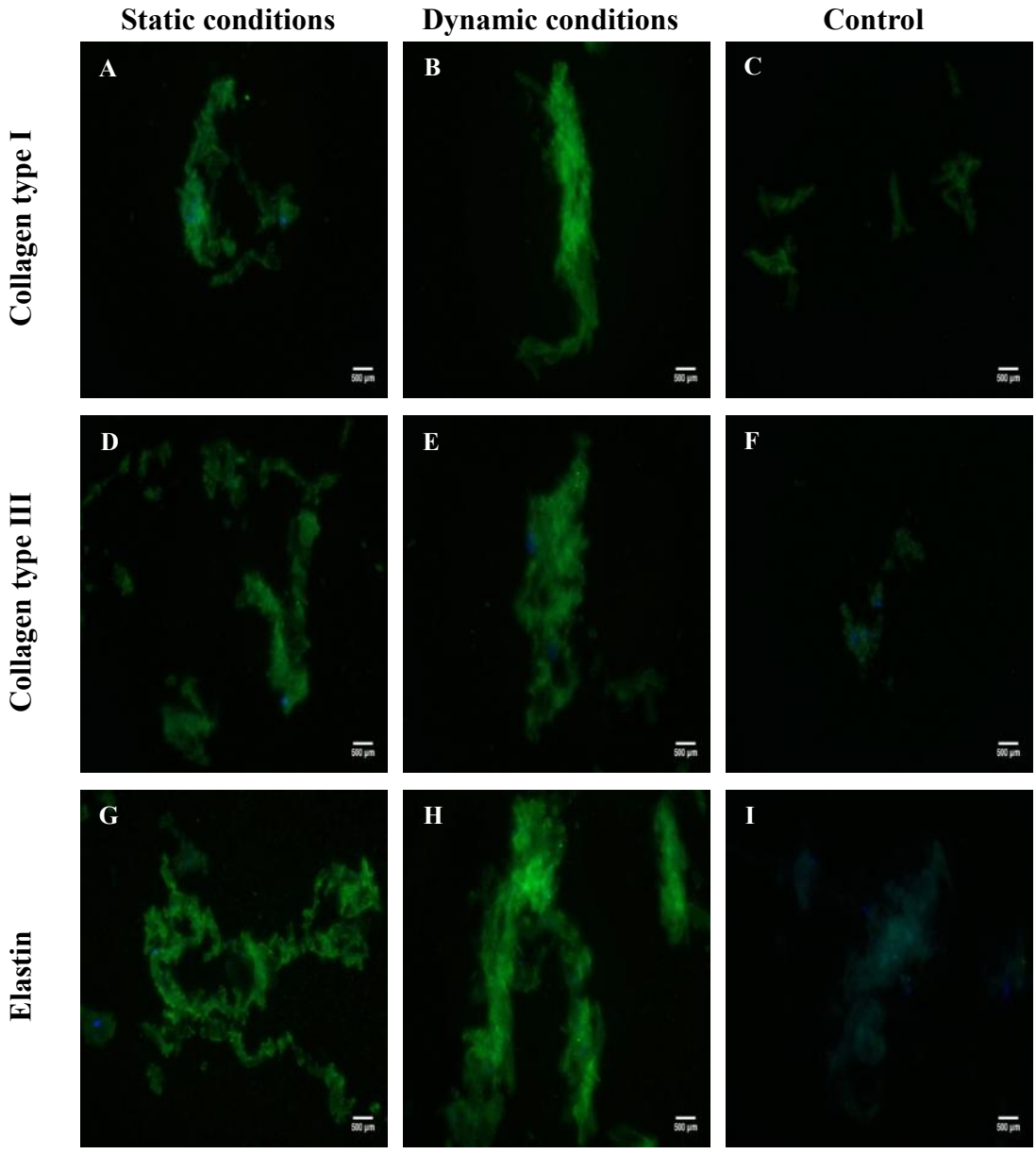

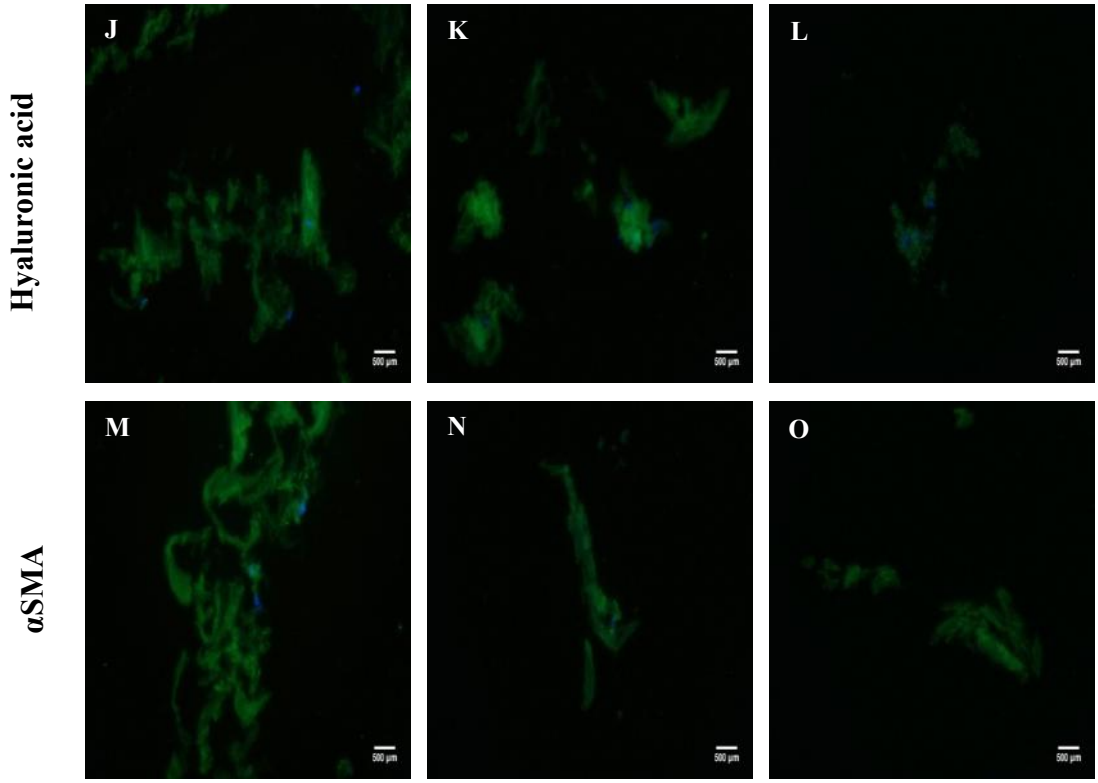

Figure 26 Fibroblasts seeded into fibers mounted on culture-inserts using the optimized method and accordingly stained for (A) collagen type I detection under static conditions at 20x magnification, (B) collagen type I detection under dynamic conditions at 20x magnification, (C) mouse control detection where the primary antibody was excluded at 20x magnification, (D) collagen type III detection under static conditions at 20x magnification, (E) collagen type III detection under dynamic conditions at 20x magnification, (F) rabbit control detection where the primary antibody was excluded at 20x magnification, (G) elastin detection under static conditions at 20x magnification, (H) elastin detection under dynamic conditions at 20x magnification, (I) guinea pig control detection where the primary antibody was excluded at 20x magnification, (J) hyaluronic acid detection under static conditions at 20x magnification, (K) hyaluronic acid detection under dynamic conditions at 20x magnification, (L) rabbit control detection where the primary antibody was excluded at 20x magnification, (M) αSMA detection under static conditions at 20x magnification, (N) αSMA detection under dynamic conditions at 20x magnification, and (O) rabbit control detection where the primary antibody was excluded at 20x magnification. Nuclei were stained with DAPI (blue) (A – O).

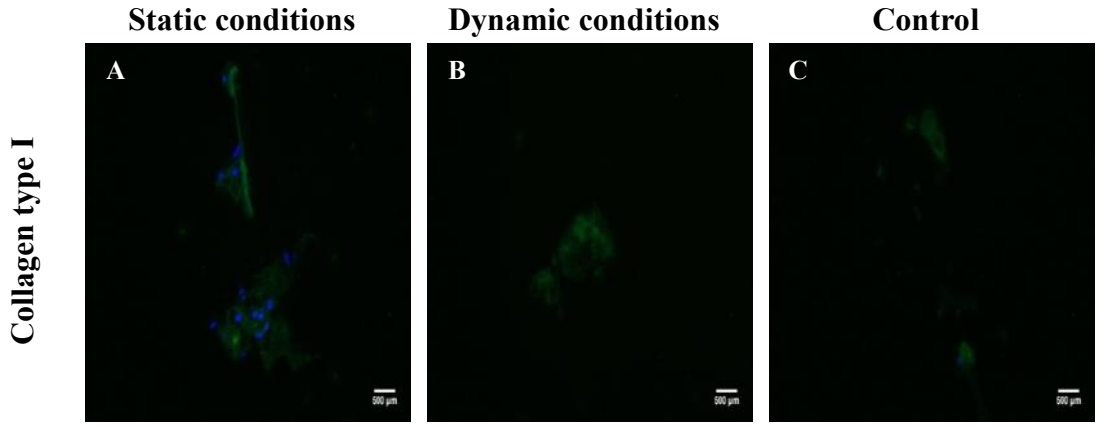

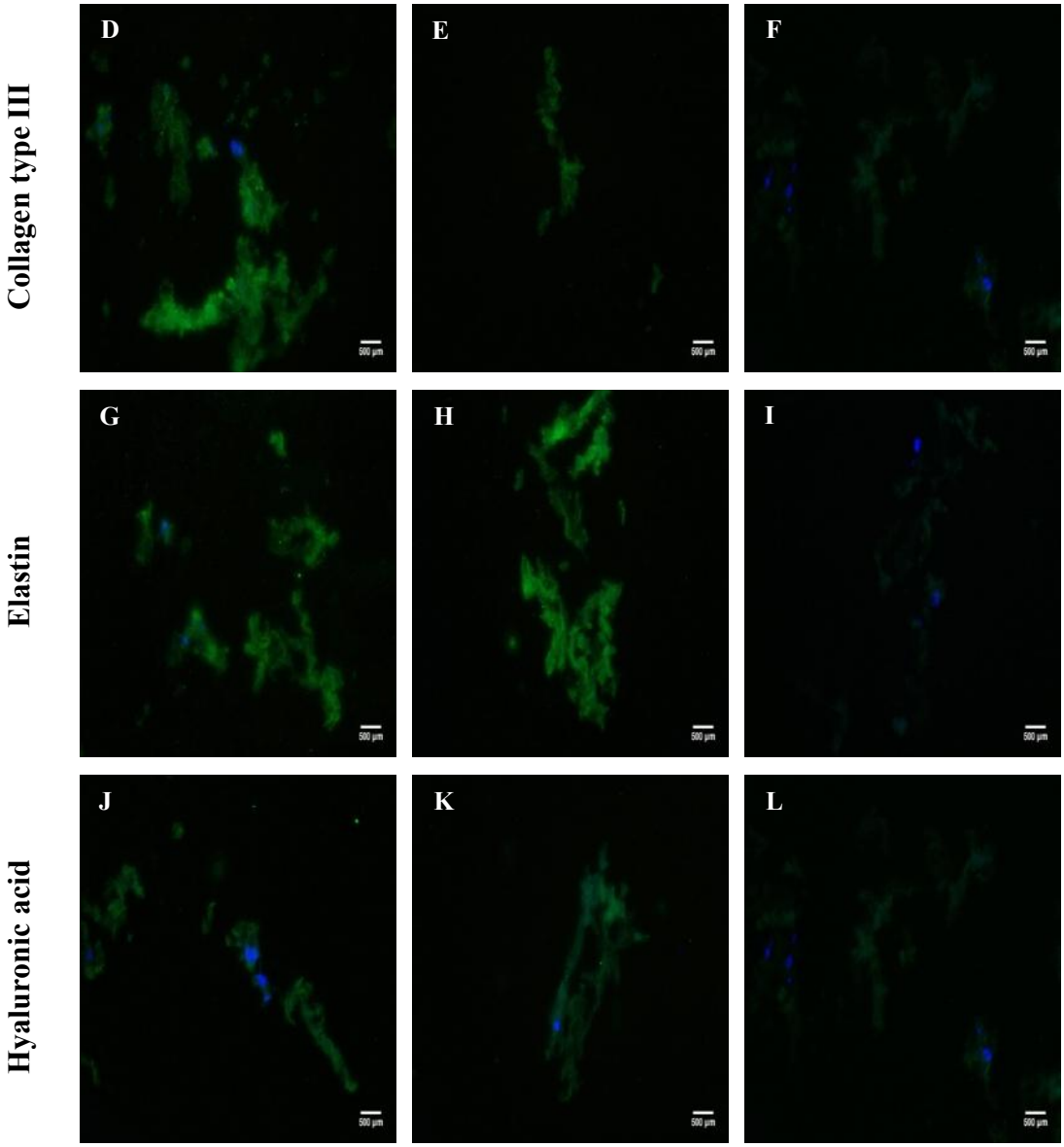

Figure 27 Endothelial cells seeded into fibers mounted on culture-inserts using the optimized method and accordingly stained for (A) collagen type I detection under static conditions at 20x magnification, (B) collagen type I detection under dynamic conditions at 20x magnification, (C) mouse control detection where the primary antibody was excluded at 20x magnification, (D) collagen type III detection under static conditions at 20x magnification, (E) collagen type III detection under dynamic conditions at 20x magnification, (F) rabbit control detection where the primary antibody was excluded at 20x magnification, (G) elastin detection under static conditions at 20x magnification, (H) elastin detection under dynamic conditions at 20x magnification, (I) guinea pig control detection where the primary antibody was excluded at 20x magnification, (J) hyaluronic acid detection under static conditions at 20x magnification, (K) hyaluronic acid detection under dynamic conditions at 20x magnification, (L) rabbit control detection where the primary antibody was excluded at 20x magnification. Nuclei were stained with DAPI (blue) (A – L).

3.4 Hematoxylin and eosin staining

Silk foams and fibers - Non-optimized approach. In order to further investigate cell viability and dispersion of hDFn and hUVECs into the protein-made matrices, sections were accordingly stained with hematoxylin and eosin (Figure 28). Images

captured under the bright field microscope confirmed the presence of both cell types and in addition, revealed a well-arranged cell distribution inside the scaffolds.

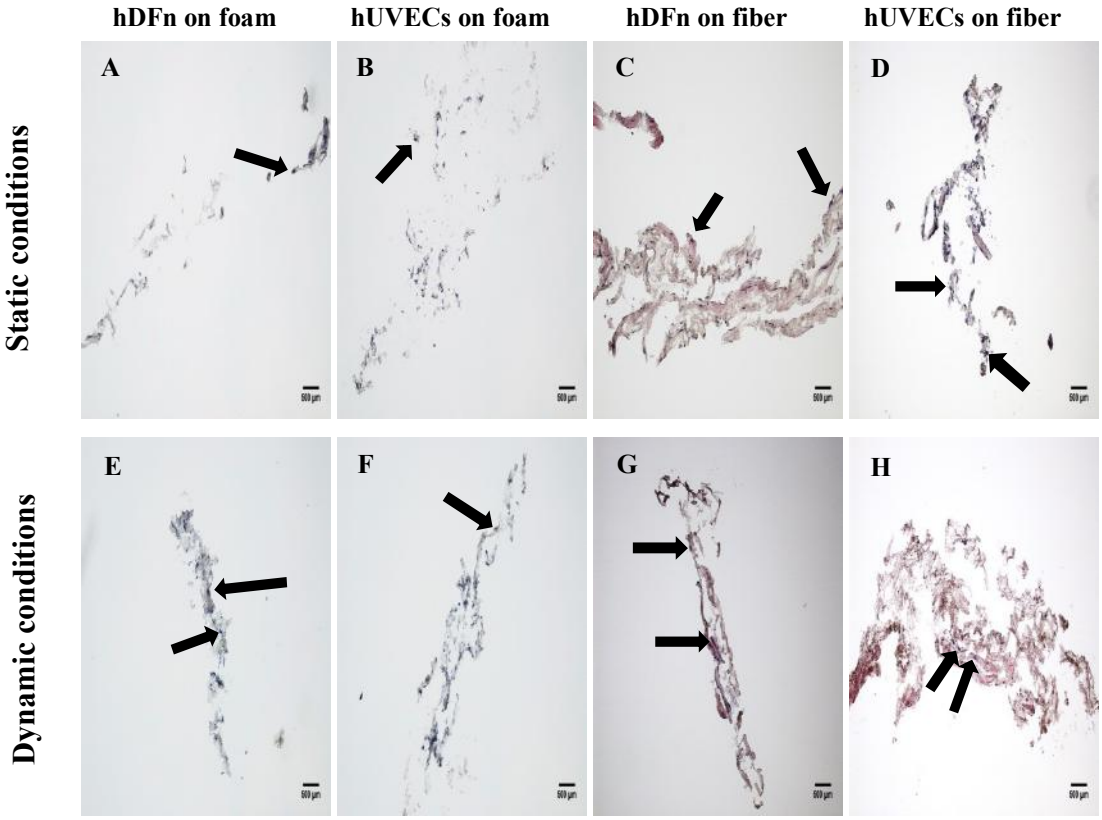

Figure 28 Hematoxylin and eosin staining of (A) hDFn on foam under static conditions at 10x magnification, (B) hUVECs on foam under static conditions at 10x magnification, (C) hDFn on fiber under static conditions at 10x magnification, (D) hUVECs on fiber under static conditions at 10x magnification, (E) hDFn on foam under dynamic conditions at 10x magnification, (F) hUVECs on foam under dynamic conditions at 10x magnification, (G) hDFn on fiber under dynamic conditions at 10x magnification, and (H) hUVECs on fiber under dynamic conditions at 10x magnification. Hematoxylin (dark blue dots - pointed by black arrows) was introduced to stain cell nuclei, whereas eosin (pink color) was used to stain the protein sections.

Optimized fiber mounting. Similarly to the non-optimized approach, cell viability and distribution of cells seeded into the protein-made fibers mounted using the optimized method was also investigated. Sections were also accordingly stained with hematoxylin and eosin. Images captured under the bright field microscope (Figure 29) confirmed to a lesser or greater extent the findings which were observed in the non-optimized approach.

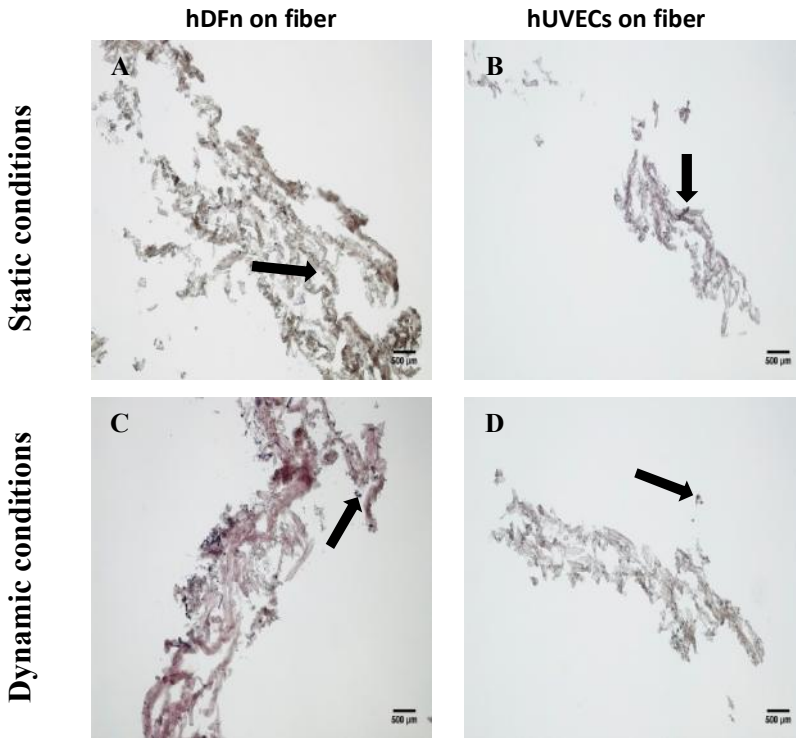

Figure 29 Hematoxylin and eosin staining of (A) hDFn under static conditions at 10x magnification, (B) hUVECs under static conditions at 10x magnification, (C) hDFn under dynamic conditions at 10x magnification, (D) hUVECs under dynamic conditions at 10x magnification. Hematoxylin (dark blue dots - pointed by black arrows) was introduced to stain cell nuclei, whereas eosin (pink color) was used to stain the protein sections.

3.5 Quantification analysis on protein coatings

At last, immunofluorescence images captured on protein-coated cover slips were further analyzed in order to provide comparable information between the two differently conditioned cell types. As collagen type III and elastin were the sole proteins largely detected on WT and FN variants, they were strongly considered for quantifying their respective secreted amounts.

Results indicated that the statically conditioned fibroblasts and endothelial cells were slightly less secretory in the structural components analyzed, in comparison to the respective cells exposed to shear stresses (Figures 30, 31, 32, and 33). Nonetheless, more measurement values were required for statistical analysis to be performed.

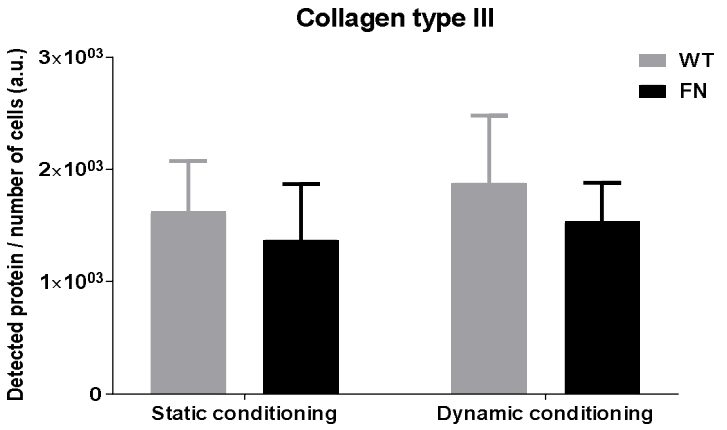

Figure 30 Quantification of detected collagen type III on hDFn seeded onto the WT and FN silk variants exposed to both conditions. The y axis represents the ratio between the total area of pixel intensity values belonging to detected protein and the number of cells on the nine separate fluorescence images taken over each cover slip. Mean values have been calculated and plotted. Error bars represent maximum values from standard deviation.

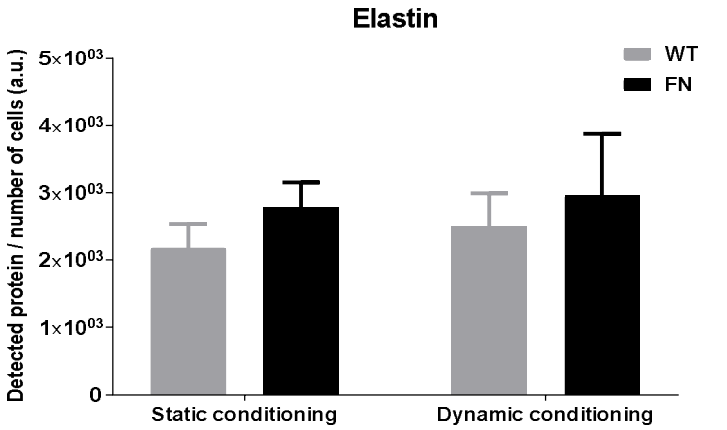

Figure 31 Quantification of detected elastin on hDFn seeded onto the WT and FN silk variants exposed to both conditions. The y axis represents the ratio between the total area of pixel intensity values belonging to detected protein and the number of cells on the nine separate fluorescence images taken over each cover slip. Mean values have been calculated and plotted. Error bars represent maximum values from standard deviation.

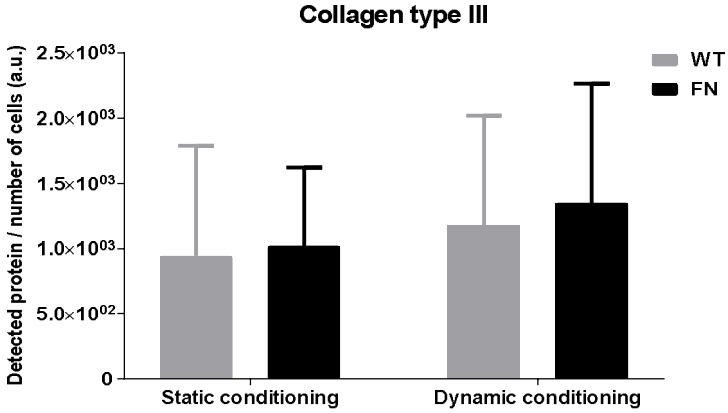

Figure 32 Quantification of detected collagen type III on hUVECs seeded onto the WT and FN silk variants and exposed to both conditions. The y axis represents the ratio between the total area of pixel intensity values belonging to detected protein and the number of cells on the nine separate

fluorescence images taken over each cover slip. Mean values have been calculated and plotted. Error bars represent maximum values from standard deviation.

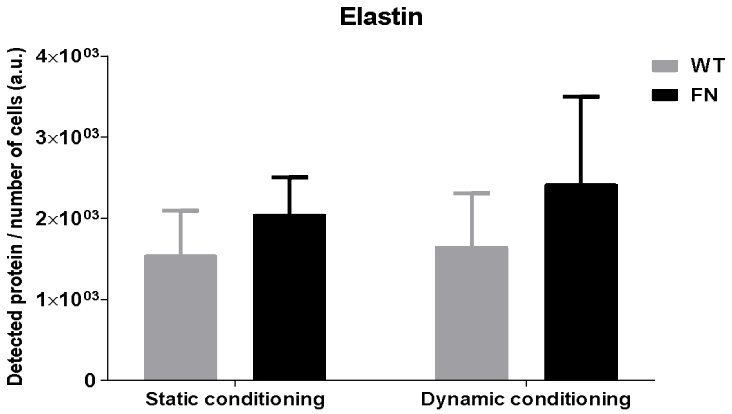

Figure 33 Quantification of detected elastin on hUVECs seeded onto the WT and FN silk variants exposed to both conditions. The y axis represents the ratio between the total area of pixel intensity values belonging to detected protein and the number of cells on the nine separate fluorescence images taken over each cover slip. Mean values have been calculated and plotted. Error bars represent maximum values from standard deviation.

Finally, the increase in secreted amount of proteins by the dynamically conditioned hDFn and hUVECs onto the silk variants, as compared to the respective cultured under static conditions, has been collectively summed up in the following table 6. Values were obtained as explained in the materials and methods section.

Table 6 The increase in percentage (%) of protein secretion by the dynamically conditioned cell types seeded onto the WT and FN silk variants, as compared to the respective cultured under static conditioning.

Protein	hDFn on WT	hDFn on FN	hUVECs on WT	hUVECs on FN
Collagen type III	14.40	11.37	22.18	27.97
Elastin	13.63	6.40	6.24	17.09

4 Discussion

In the current study, partial spider silk utilized to coat surfaces as well as configured into 3D matrices was extensively assessed as the scaffold to be potentially used in tissue engineering the aortic cusp milieu. In general, the evaluation process indicated that both cell types seeded onto the protein coatings as well as into the foam and fiber constructs responded to vigorous fluid dynamics; innately generated in native tissue. More precisely, the silk protein was shown to facilitate cell adhesion and proliferation and most importantly, secretion of tissue-specific compounds, which can be attributed to cell compliance with host material.

In particular, protein-coated well surfaces facilitated to a great extent cell adhesion of fibroblasts and endothelial cells as well as promoted cellular growth after cell-seeding. Bright field images captured on stained cells with the Crystal Violet assay (Figures 5 and 6) demonstrated also significant increase in cell numbers between 24 and 48 hours following the seeding process. Additionally, the typical cell morphology for each respective cell type was confirmed as well. Images illustrated fibroblasts to have developed an elongated morphology with several anchoring points to the protein-coated substrates. Fibroblasts are commonly derived from mesenchymal stem cells or multipotent progenitor cells and during cardiac tissue's developmental process, they become well arranged in sheets and strands displaying a typical flattened – elongated morphology [78,79]. Human umbilical vein endothelial cells on the other hand exhibited the characteristic cobblestone-like morphology related to the endothelium phenotype [80] and as previously reported [81], implied profound cell adherence to protein substrate. In comparison to the respective WT, well surfaces coated with the FN variant were shown to promote cell adhesion and proliferation in a higher degree. It has been previously found [70,71] that the RGD motif promotes early cell adherence, which can further be confirmed by the noticeable spread-out morphology of fibroblasts onto the FN variant 24 hours post cell-seeding (Figure 5G).

Cell viability and growth rate results more concretely support the aforementioned observations, as both cell types seeded onto the protein coatings and 3D matrices were shown to remarkably proliferate throughout the complete experimentation. More specifically, fibroblasts as well as endothelial cells onto the protein-coated cover slips displayed a gradual growth profile and more precisely, reached higher figures under the dynamic conditions prior to cell fixation. Until fixation day though, the growth between the two anisotropically conditioned fibroblasts (Figure 7) was not considerably different, thereby confirming that fibroblasts do not as willingly as other cell types proliferate in response to low shear stresses [82]. On the contrary, hUVECs cultured under the dynamic conditions (Figure 8) exhibited a more linearly-related growth rate, highlighting the evidence that the endothelium needs to be exposed to reciprocating shear stresses over the same place for low-lasting periods of time [83]. More interestingly though, on both cases cells seeded onto the non-pre-coated (controls) cover slips were shown to proliferate in a higher extent under the static conditions. This particular observation explains the necessity of cells to be adhered to a sturdy substrate when exposed to mechanical stimuli. Dynamically conditioned cells onto controls therefore might have been started to become apoptotic or cell growth might have been hindered in the absence of a solid matrix to support cell viability.

Concomitant with findings on cell-seeded protein coatings, fibroblasts as well as endothelial cells into the protein-made foam constructs demonstrated similar proliferative behavior when subjected to fluid dynamics. More precisely, both cell types were attributed to a linear growth and reached to a lesser or greater extent similar figures prior to cell fixation (Figures 9 and 10). An obvious difference in cell

proliferation as compared to the statically conditioned cells was also noticed, thereby further crediting the belief that the silk can be regarded a sustainable scaffold. Unexpectedly though, fluorescence intensity values obtained and subsequently processed on cell-seeded protein-made fibers reported contradictory results, as compared to the respective on foam matrices. Fibroblasts as well as endothelial cells into the fibers were shown to more rapidly proliferate under the static conditions in contrast to the respective under the dynamic ones (Figures 11 and 12). The unexpected irregularity can be explained by the differently sized pieces of fibers (2 - 3 cm) mounted on culture-inserts and intended for dynamic conditioning. As a matter of fact, cell-seeded fibers subjected to static conditions were much longer (4 - 5 cm) and thereby, fibroblasts as well as endothelial cells were provided a more outspread matrix to grow in and proliferate. In addition, the amount of cells that ultimately manage to adhere to the protein during fiber formation is highly random and thereby, the outcome in cell proliferation might be considerably questionable. It can thus be concluded that the cell-seeded fiber matrices subjected to shear stresses displayed a sufficient cell growth on both cell types seeded, which would have been otherwise similar to the proliferation in foam constructs under the dynamic conditions. To better comprehend cell viability into protein-made fibers, cell-seeded matrices can ideally be stained with the Alamar Blue assay and according to the results acquired, similarly mounted prior to be exposed to any of the two conditions.

The optimized fiber mounting aimed in providing more comparable information regarding cell viability and growth rate under both the static and dynamic conditions. Equally sized pieces were therefore cut and mounted on culture-inserts prior to be exposed to any of them. Despite the optimized approach, a concrete conclusion cannot be ultimately drawn as results on the two anisotropically conditioned cell-seeded fiber pieces contradict. It can be speculated though that the fibroblasts populated the piece of fiber which was statically conditioned (Figure 13) didn't grow as intended due to poor mounting on culture-insert. In fact, the fiber became loose touching the insert's walls and thereby, cells might have been started to become apoptotic after culture day 2. On the other hand, the endothelial cell-seeded piece of fiber that was subjected to dynamic conditions (Figure 14) must have been highly likely deprived of an adequate amount of cells in the first place, which would have resulted in a significant cell growth later on. To be in a better position to have drawn conclusions from the optimized fiber study, a substantially larger number of fibers was inevitably needed to be subjected to both conditions.

As described above, the ECM composition of the aortic cusp milieu in structural components is highly specific in order to allow the unobstructed opening and closing function of the valve. The collagen rich fibrosa crimps to keep the valvular orifice open during systole, while the elastin sheets on ventricularis firmly shut the leaflets in each diastole. The spongiosa mainly composed of non-sulfated hyaluronic acid and chondroitin sulfate acts as a shock absorber and lubricates the complex tissue. One

can understand hence that the secretion of tissue-specific compounds should be as highly as possible promoted by the cell-seeded scaffold in tissue engineering approaches.

Throughout the entire experimentation, both cell types examined on protein coatings and 3D matrices were strongly shown to synthesize elastin in large amounts. Most interestingly, fibroblasts as well as endothelial cells onto the dynamically conditioned protein-coated cover slips displayed an increased inclination in elastin composition (Table 6). Unfortunately, quantification analysis in elastin synthesis by the anisotropically conditioned cell types was difficult to be performed in the protein-made scaffolds. The fluorescent signal induced by the foam and fiber pieces themselves did not allow the same technique to be applied, as in the case of protein coatings. In addition, the exact number of cells found into the sectioned matrices was rather hard to be accurately specified. The same etiology applies for the rest of the detected proteins as well. Immunofluorescence images captured though on accordingly stained sections undoubtedly confirmed elastin's presence in large deposits (Figures 22I, 22K, 23I, 23K, 24I, 24K, 25I, 25K, 26G, 26H, 27G, and 27H).

Further, an extensive fibrous network formation of extracellularly deposited collagen type III on protein coatings was notably observed on both cell types seeded and accordingly conditioned (Figures 15A, 15C, 15E, 15G, 19A, 19C, 19E, and 19G). In fact, both cell types analyzed were shown to be highly prone in collagen type III secretion under the shear stresses applied, denoting increased cellular response to fluid dynamics (Table 6). Similar conclusions can be to a lesser or greater extent drawn in protein-made scaffolds, as collagen type III was detected in the majority of the respectively stained sections. The most ambiguous images taken on stained sections that cannot as greatly as the rest confirm collagen's type III secretion are on seeded fibroblasts into the foam and non-optimized mounted fiber constructs (Figures 22E, 22G, 24E, and 24G). A reasonable explanation for protein's poor detection can be given by the primary antibody not having bound properly to the protein of interest or the high auto-fluorescent silk that didn't allow a clear detection.

Unfortunately, collagen type I as well as hyaluronic acid was weakly detected on the cell-seeded protein coatings (Figures 18 and 21). Fibroblasts on WT and FN silk variants were kept in expansion for a low-lasting culture period (8 days) that might have been an inadequate amount of time for hDFn to start synthesizing collagen I and hyaluronic acid in large amounts. More specifically, collagen type I synthesis is generally described as a complex and laborious process in order to be assembled into the known triple helical structure. In fact, the triple stranded assembly containing glycine and proline as the principal amino acids is initially known as procollagen, which is subsequently cleaved in the extracellular space to give rise to collagen fibrils [84]. Hyaluronic acid on the other hand is natively synthesized by a family of integral membrane proteins (IMPs) known as hyaluronan synthases. In a similarly complex process, the secondary structure of hyaluronic acid produced by the IMPs is further

assembled into the long and highly repeated disaccharide structure by the hyaluronan synthase enzymes. The enzymes are responsible to adding in an alternating fashion glucuronic acid and N-acetylglucosamine to the rapidly growing polymeric chain by making use of compounds activated nucleotide sugars as substrates [85]. On the contrary, endothelial cells have often been reported as a poor-secretory collagen type I cell source when cultured in vitro [86,87]. The absence of detectable collagen type I in any of the endothelial cell-seeded protein-coated cover slips as well as 3D matrices can hence be explained. In contrast to protein coatings, collagen type I was indeed detected on fluorescently labeled fibroblasts into the foam (Figures 22A and 22C) as well as into the optimized mounted fiber (Figures 26A and 26B) constructs. In addition, fluid dynamics in cell-seeded foam and fiber scaffolds must have driven hDFn and hUVECs to synthesize hyaluronic acid, as respective fluorescence images captured (Figures 22O, 23O, 24O, 25O, and 26K) portrayed an obvious difference when compared to the respectively taken on the statically conditioned cells. It has been previously reported [85] that HA when used to coat biomaterial surfaces is exceptionally competent in preventing platelet adhesion and thereby, potential thrombi formation. Foam and fiber matrices can thus be considered greatly indicative to tissue engineer the cardiovasculature, given the facilitation in hyaluronic acid synthesis under dynamic conditioning.

Further, the differentiation of fibroblasts into myofibroblasts was confirmed on both the protein-coated cover slips (Figure 17), as stained cells for αSMA detection were positively fluoresced. It has been recently shown [78,88] that treatment of fibroblasts with the TGF-β factor results in elevated collagen synthesis as a consequence of the myofibroblast phenotype. The supposed differentiation into the protein-made 3D matrices can hence be assumed, as the fluorescence images captured on either the statically (Figures 22Q, 24Q, and 26M) or dynamically (Figures 22S, 24S, and 26N) conditioned fibroblasts cannot entirely let any convincing conclusion to be drawn. To more concretely confirm the differentiation into myofibroblasts, hDFn seeded into the protein-made foam and fiber scaffolds could have been also stained for vimentin expression [88].

At last, hematoxylin and eosin stainings performed on sectioned foam and fiber constructs (Figure 28) as well as fibers mounted using the optimized method (Figure 29) also confirmed cell viability. Images captured under the bright field microscope to a lesser or greater extent indicated a well dispersed cellular presence over the silk matrices. Observations made are correlated to Alamar Blue assay findings, thereby further crediting the belief that the silk can sufficiently promote cellular growth when configured into various formats [64].

Admittedly, partial spider silk has opened a wide range of potential application areas where sound mechanical properties are highly required. The complex functionality as well as continuous operation of the aortic valve tissue constitutes such a circumstance. Herein, both the wild type and respective functionalized silk variants

were thoroughly examined and shown great promise to be used in tissue engineering the aortic valve. Protein coatings displayed a profound cell viability and growth rate and additionally, demonstrated adequate competence in cell secretion of tissue-specific compounds by seeded cells. Moreover, the differentiation of fibroblasts into myofibroblasts was also supported by the protein. In parallel to those observations, cell viability and proliferation was also established in the protein-made 3D scaffolds and most importantly, secretion of essential compounds could be confirmed as well.

In general, an increased tendency in cell growth as well as protein deposition was noticed on both cell types seeded onto the protein-coated substrates and into the 3D matrices subjected to vigorous fluid dynamics. It can hence be assumed that the seeded cells not only responded to mechanical stimuli but also synthesized even more structural components to compensate for them. As a matter of fact, the functionalized silk variant facilitated cell adhesion and proliferation in a higher degree as compared to the respective wild type. Most interestingly, quantification analysis revealed that the endothelial cells on the FN variant were highly secretory in collagen type III and elastin, whereas fibroblasts only in elastin, as compared to the respective WT. Partial spider silk coupled with the fibronectin mimetic motif has been previously reported [71] to have been successfully assembled into stable matrices and most importantly, to have supported cell adherence and improved cell viability. The functionalized silk variant can thus be regarded more indicative in similar tissue engineering approaches due to the motif that acts as a cell attraction site and further drives subsequent biological responses.

Future studies are required nevertheless to put into scrutiny the mechanical properties as well as the overall biomechanics behavior of cell-seeded foam and fiber constructs. As it has not been evaluated yet, a stress-strain test along with a fatigue process in protein-made and cell-seeded foam and fiber scaffolds will further elucidate the protein's integrity and stability after deposition of structural components. Moreover, the question of whether it can be potentially implanted as an aortic valve substitute will possibly be addressed. So far, spider silk has little been evaluated in vivo, mainly as a wound dressing [73,89], in peripheral nerve regeneration [90], and as an implant in general [74]. It is thereby challenging to be assessed in a highly demanding environment, such as the aortic valve's, given the promising results obtained by the dynamically conditioned hDFn and hUVECs onto the protein coatings as well as into the 3D matrices.

5 Conclusion

Herein, partial spider silk was extensively assessed in terms of cell adhesion, cell proliferation, and tissue-specific protein secretion. Three separate experimental setups involved the incorporation of human dermal fibroblasts as well as human umbilical

vein endothelial cells onto protein-coated substrates and protein-made matrices. Cell-seeded coatings and 3D scaffolds were further exposed to static as well as dynamic conditions. The protein was conclusively shown to have facilitated cell adhesion and cell growth and more importantly, enable cells in elevated protein secretion under the shear stresses applied. In addition, silk protein was reported to have successfully supported the differentiation of fibroblasts into myofibroblasts. To sum up, recombinantly synthesized spider silk holds great promise to be used as the scaffold to tissue engineer the aortic valve and further evaluated in vivo.

6 Acknowledgements

I would like to express my sincere gratitude to My Hedhammar for having accepted my master thesis project proposal and allowing me to work in a tremendously exciting subject. I also express my deepest sympathies to Mona Widhe for being a wonderful person and an excellent supervisor. I would like to also kindly thank Spiber Technologies for its generosity to provide all the necessary silk protein used and Tomas Rosén for the lego-vagga wave-rocking platform. I am also greatly thankful to Julie Gold for being an inspiring professor in the tissue engineering field and Mr. Ioannis Loukos for continuously supporting me to pursue master's degree knowledge. Most importantly, I am more than grateful to my parents, Giorgos and Konstantina, and my brother, Lambros, for all the moral and ethical values offered, as well as all the financial contribution granted throughout those years. Last but not least, I am greatly thankful to Mihaela for having changed and being in my life. This study would have not been possible without them. Thank you.

7 References

[1] Fedak, P.W.M., et al., *Clinical and Pathophysiological Implications of a Bicuspid Aortic Valve.* Circulation, 2002. **106**: p. 900-904.

[2] Baliga, R.R., et al., in *Practical Cardiology*. 2008, Lippincott Williams & Wilkins. p. 452.

[3] Hasan, A., et al., *Biomechanical properties of native and tissue engineered heart valve constructs.* Journal of Biomechanics, 2014. **47**: p. 1949-1963.

[4] El-Hamamsy, I., A.H. Chester, and M.H. Yacoub, *Cellular regulation of the structure and function of aortic valves.* Journal of Advanced Research, 2010. **1**: p. 5-12.

[5] Leopold, J.A., *Cellular Mechanisms of Aortic Valve Calcification.* Basic Science for Clinicians, 2012. **5**: p. 605-614.

[6] Filová, E., et al., *Tissue-Engineered Heart Valves.* Physiological Research, 2009. **58**: p. 141-158.

[7] Latif, N., et al., *Localization and Pattern of Expression of Extracellular Matrix Components in Human Heart Valves* The journal of heart valve disease, 2005. **14**(2): p. 1-10.

[8] Jana, S., R.T. Tranquillo, and A. Lerman, *Cells for tissue engineering of cardiac valves.* Journal of tissue engineering and regenerative medicine, 2015.

[9] Schoen, F.J., *Evolving Concepts of Cardiac Valve Dyamics - The Continuum of Development, Functional Structure, Pathobiology, and Tissue Engineering.* Circulation, 2008. **118**: p. 1864-1880.

[10] Yap, C.H., N. Saikrishnan, and A.P. Yoganathan, *Experimental measurement of dynamic fluid shear stress on the ventricular surface of the aortic valve leaflet.* Biomech Model Mechanobiol., 2012. **11**: p. 231-244.

[11] Yap, C.H., et al., *Experimental measurement of dynamic fluid shear stress on the aortic surface of the aortic valve leaflet.* Biomech Model Mechanobiol., 2012. **11**: p. 171-182.

[12] Stradins, P., et al., *Comparison of biomechanical and structural properties between human aortic and pulmonary valve.* European Journal of Cardio-thoracic Surgery, 2004. **26**: p. 634-639.

[13] Balguid, A., et al., *The role of collagen cross-links in biomechanical behavior of human aortic heart valve leaflets - Relevance for tissue engineering.* Tissue Engineering, 2007. **13**: p. 1501-1511.

[14] Maganti, K., et al., *Valvular Heart Disease: Diagnosis and Management.* Mayo Clinic Proceedings, 2010. **85**(5): p. 483-500.

[15] Bonow, R.O., et al., *Valvular heart disease*, in *Braunwald's Heart Disease: A Textbook of Cardio-vascular Medicine*. 2007, WB Saunders: Philadelphia. p. 1625-1712.

[16] Ross , J.J. and E. Braunwald, *Aortic stenosis.* Circulation, 1968. **38**(1): p. 61-67.

[17] Bhandari, S., K. Suramanyam, and N. Trehan, *Valvular Heart Disease: Diagnosis and Management.* Japi, 2007. **55**: p. 575-584.

[18] Rajamannan, N., *Calcific aortic stenosis: lessons learned from experimental and clinical studies.* Arteriosclerosis, thrombosis and vascular biology, 2009. **29**(2): p. 162-168.

[19] Mol, A., et al., *Tissue engineering of heart valves: advances and current challenges.* Expert Review Medical Devices, 2009. **6**(3): p. 259-275.

[20] Agabegi, E.D. and S.S. Agabegi, *Diseases of the Cardiovascular system - Valvular Heart Disease*, in *Step-Up to Medicine*, W. Kluwer, Editor. 2008, Lippincott Williams & Wilkins: Baltimore.

[21] Pibarot, P. and J.G. Dumesnil, *Prosthetic Heart Valves - Selection of the Optimal Prosthesis and Long-Term Management.* Circulation, 2009. **119**: p. 1034-1048.

[22] Mykén, P.S., *Medscape*. 2006.

[23] Brown, J.M., et al., *Isolated aortic valve replacement in North America comprising 108,687 patients in 10 years: Changes in risks, valve types, and outcomes in the Society of Thoracic Surgeons National Database.* The Journal of Thoracic and Cardiovascular Surgery, 2009. **137**(1): p. 82-90.

[24] Friberg, Ö., et al., *Swedish Heart Surgery Registry*. 2014: Stockholm.

[25] Geller, C.M., *Mount Sinai Beth Israel*. 2016.

[26] Raiten, J., *Anticoagulation Therapy Following Embolic or Hemorrhagic Stroke in the Patient with a Mechanical Heart Valve.* Journal of Anesthesia & Clinical Research, 2011. **2**(9): p. 1-3.

[27] Golczyk, K., et al., *Heart Valve Sound of Various Mechanical Composite Grafts, and the Impact on Patients' Quality of Life.* The Journal of heart valve disease, 2010. **19**(2): p. 228-232.

[28] Vesely, I., *Heart Valve Tissue Engineering.* Circulation Research, 2005. **97**: p. 743-755.

[29] Delmo Walter, E.M., et al., *The future of heart valve banking and of homografts: perspective from the Deutsches Herzzentrum Berlin.* HSR Proceedings in Intensive Care and Cardiovascular Anesthesia, 2012. **4**(2): p. 97-108.

[30] Hoffmann, G., G. Lutter, and J. Cremer, *Durability of Bioprosthetic Cardiac Valves.* Deutsches Ärzteblatt International, 2008. **105**(8): p. 143-148.

[31] Yacoub, M., et al., *An evaluation of the Ross operation in adults.* Journal of Heart Valve Disease, 2006. **15**(4): p. 531-539.

[32] Assadi, R., et al., *Medscape*. 2015.

[33] Rippel, R.A., H. Ghanbari, and A.M. Seifalian, *Tissue-Engineered Heart Valve: Future of Cardiac Surgery.* World Journal of Surgery, 2012. **36**: p. 1581-1591.

[34] Bloch, O., et al., *Immune Response in Patients Receiving a Bioprosthetic Heart Valve: Lack of Response with Decellularized Valves.* Tissue Engineering: Part A, 2011. **17**(19-20): p. 2399-2405.

[35] Kasimir, M.-T., et al., *The decellularized porcine heart valve matrix in tissue engineering.* Thromb Haemost, 2005. **94**: p. 562-567.

[36] Lee, C.H., A. Singla, and Y. Lee, *Biomdecial applications of collagen.* International Journal of Pharmaceutics, 2001. **221**(1-2): p. 1-22.

[37] Daamen, W.F., et al., *Elastin as a biomaterial for tissue engineering.* Biomaterials, 2007. **28**(30): p. 4378-4398.

[38] Tedder, M.E., et al., *Stabilized Collagen Scaffolds for Heart Valve Tissue Engineering.* Tissue Engineering: Part A, 2009. **15**(6): p. 1257-1268.

[39] Mendelson, K. and F.J. Schoen, *Heart Valve Tissue Engineering: Concepts, Approaches, Progress and Challenges* Annals of Biomedical Engineering, 2006. **34**(12): p. 1799-1819.

[40] Kohn, J., S. Abramson, and R. Langer, *Bioresorbable and bioerodible materials*, in *Biomaterials Science: An Introduction to Materials in Medicine*, B.D. Ratner, et al., Editors. 2004, Academic Press: Orlando.

[41] Schmidt, D. and S.P. Hoerstrup, *Tissue engineered heart valves based on human cells* Swiss Medical Weekly, 2005. **135**: p. 618-623.

[42] Smith, S., et al., *Force Generation of Different Human Cardiac Valve Interstitial Cells: Relevance to Individual Valve Function and Tissue Engineering.* The Journal of Heart Valve Disease, 2007. **16**(4): p. 440-446.

[43] Narine, K., et al., *Transforming growth factor-beta-induced transition of fibroblasts: a model for myofibroblast procurement in tissue valve engineering.* The Journal of heart valve disease, 2004. **13**(2): p. 281-289.

[44] Sukmana, I. and P. Vermette, *The effects of co-culture with fibroblasts and angiogenic growth factors on microvascular maturation and multi-cellular lumen formation in HUVEC-oriented polymer fibre constructs.* Biomaterials, 2010. **31**: p. 5091-5099.

[45] Weymann, A., et al., *Reendothelialization of Human Heart Valve Neoscaffolds Using Umbilical Cord-Derived Endothelial Cells.* Circulation Journal, 2013. **77**: p. 207-216.

[46] Bischoff, J. and E. Aikawa, *Progenitor Cells Confer Plasticity to Cardiac Valve Endothelium.* Journal of Cardiovascular Translational Research, 2011. **4**(6): p. 710-719.

[47] Wang, H.-S., et al., *Mesenchymal Stem Cells in the Wharton's Jelly of the Human Umbilical Cord.* Stem Cells, 2004. **22**(7): p. 1330-1337.

[48] Knight, R., et al., *Tissue engineering of cardiac valves: re-seeding of acellular porcine aortic valve matrices with human mesenchymal progenitor cells.* Journal of heart valve disease, 2005. **14**(6): p. 806-813.

[49] Colazzo, F., et al., *Extracellular matrix production by adipose-derived stem cells: Implications for heart valve tissue engineering.* Biomaterials, 2011. **32**(1): p. 119-127.

[50] Tucker, R.P., et al., *See-saw rocking: an in vitro model for mechanotransduction research.* Journal of the Royal Society Interface 2014. **11**: p. 1-9.

[51] Aleksieva, G., et al., *Use of a special bioreactor for the cultivation of a new flexible polyurethane scaffold for aortic valve tissue engineering.* BioMedical Engineering OnLine, 2012. **11**(92): p. 1-11.

[52] Sun, L., N.M. Rajamannan, and P. Sucosky, *Design and Validation of a Novel Bioreactor to Subject Aortic Valve Leaflets to Side-Specific Shear Stress.* Annals of Biomedical Engineering, 2011. **39**(8): p. 2174-2185.

[53] Patel, A., et al., *Elastin biosynthesis: The missing link in tissue-engineered blood vessels.* Cardiovascular Research, 2006. **71**: p. 40-49.

[54] Tokareva, O., et al., *Recombinant DNA production of spider silk proteins.* Microbial Biotechnology, 2013. **6**(6): p. 651-663.

[55] Kluge, J.A., et al., *Spider silks and their applications.* Trends in Biotechnology, 2008. **26**(5): p. 244-251.

[56] Stark, M., et al., *Macroscopic Fibers Self-Assembled from Recombinant Miniature Spider Silk Proteins.* Biomacromolecules, 2007. **8**(5): p. 1695-1701.

[57] Scheller, J., et al., *Purification of spider silk-elastin from transgenic plants and application for human chondrocyte proliferation.* Transgenic research, 2004. **13**(1): p. 51-57.

[58] Bini, E., et al., *RGD-Functionalized Bioengineered Spider Dragline Silk Biomaterial.* Biomacromolecules, 2006. **7**(11): p. 3139-3145.

[59] Metwalli, E., et al., *Structural changes of thin films from recombinant spider silk proteins upon post-treatment.* Applied Physics A, 2007. **89**(3): p. 655-661.

[60] Liebmann, B., et al., *Formulation of poorly water-soluble substances using self-assembling spider silk protein.* Colloids and Surfaces A: Physicochemical and Engineering Aspects, 2008. **331**(1-2): p. 126-132.

[61] Lammel, A., et al., *Processing Conditions for the Formation of Spider Silk Microspheres.* ChemSusChem, 2008. **1**(5): p. 413-416.

[62] Slotta, U.K., et al., *An Engineered Spider Silk Protein Forms Microspheres.* Angewandte Chemie, 2008. **47**(24): p. 4592-4594.

[63] Agapov, I.I., et al., *Three-dimensional scaffold made from recombinant spider silk protein for tissue engineering.* Biochemistry, Biophysics, And Molecular Biology, 2009. **426**(1): p. 127-130.

[64] Widhe , M., et al., *Recombinant spider silk as matrices for cell culture.* Biomaterials, 2010. **31**(36): p. 9575-9585.

[65] Grip, S., J. Johansson, and M. Hedhammar, *Engineered disulfides improve mechanical properties of recombinant spider silk.* Protein Science 2009. **18**: p. 1012-1022.

[66] Hedhammar, M., et al., *Sterilized Recombinant Spider Silk Fibers of Low Pyrogenicity.* Biomacromolecules, 2010. **11**(4): p. 953-959.

[67] Rising, A., et al., *Spider silk proteins: recent advances in recombinant production, structure-function relationships and biomedical applications.* Cellular and Molecular Life Sciences, 2011. **68**(2): p. 169-184.

[68] Sponner, A., et al., *Differential polymerization of the two main protein components of dragline silk during fibre spinning.* Nature Materials, 2005. **4**: p. 772-775.

[69] Wohlrab, S., et al., *Cell adhesion and proliferation on RGD-modified recombinant spider silk proteins.* Biomaterials, 2012. **33**(28): p. 6650-6659.

[70] Widhe, M., et al., *Recombinant spider silk with cell binding motifs for specific adherence of cells.* Biomaterials, 2013. **34**: p. 8223-8234.

[71] Widhe, M., N.D. Shalaly, and M. Hedhammar, *A fibronectin mimetic motif improves integrin mediated cell binding to recombinant spider silk matrices* Biomaterials, 2016. **74**: p. 256-266.

[72] Jansson, R., et al., *Recombinant Spider Silk Genetically Fucntionalized with Affinity Domains.* Biomacromolecules, 2014. **15**: p. 1696-1706.

[73] Baoyong, L., et al., *Evaluation of a new type of wound dressing made from recombinant spider silk protein using rat models.* Burns, 2010. **36**(6): p. 891-896.

[74] Fredriksson, C., et al., *Tissue Response to Subcutaneously Implanted Recombinant Spider Silk: An in Vivo Study.* Materials, 2009. **2**: p. 1908-1922.

[75] Zhou, X., et al., *Quantifying Fluid Shear Stress in a Rocking Culture Dish.* Journal of Biomechanincs, 2010. **43**(8): p. 1598-1602.

[76] Hochleitner, B.-W., et al., *Fluid Shear Stress Induces Heart Shock Protein 60 Expression in Endothelial Cells In Vitro and In Vivo.* Arteriosclerosis, Thrombosis, and Vascular Biology, 2000. **20**: p. 617-623.

[77] Delphine, D., et al., *Frictional Behavior of Individual Vascular Smooth Muscle Cells Assessed by Lateral Force Microscopy.* Materials, 2010. **3**: p. 4668-4680.

[78] Phan, S.H., *Biology of Fibroblasts and Myofibroblasts.* Annals of the American Thoracic Society, 2008. **5**: p. 334-337.

[79] Baum, J. and H.S. Duffy, *Fibroblasts and Myofibroblasts: What are we talking about?* Journal of Cardiovascular Pharmacology, 2011. **57**(4): p. 376-379.

[80] Solomon, D.E., *The seeding of human aortic endothelial cells on the extra-cellular matrix of human umbilical vein endothelial cells.* International Journal of Experimental Pathology 1992. **73**: p. 491-501.

[81] Almelkar, S., et al., *Fibrin matrix support endothelial cell adhesion and migration in culture.* OA Biology, 2014. **2**(1): p. 1-4.

[82] Joong Yull, P., et al., *Cell morphological response to low shear stress in a two-dimensional culture microsystem with magnitudes comparable to interstitial shear stress.* Biorheology, 2010. **47**: p. 165-178.

[83] White, C.R. and J.A. Frangos, *The shear stress of it all: the cell membrane and mechanochemical transduction.* Philosophical Transactions of the Royal Society, 2007. **362**: p. 1459-1467.

[84] Rishikof, D.C., et al., *Methods for Measuring Type I Collagen Synthesis In Vitro.* Methods in Molecular Medicine, 2005. **117**: p. 129-140.

[85] Necas, J., et al., *Hyaluronic acid (hyaluronan): a review.* Veterinarni Medicina, 2008. **53**(8): p. 397-411.

[86] Kay, E.P., *Expression of Types I and IV Collagen Genes in Normal and in Modulated Corneal Endothelial Cells.* Investigative Opthalmology & Visual Science, 1989. **30**(2): p. 260-268.

[87] Kusuma, S., S. Zhao, and S. Gerecht, *The extracellular matrix is a novel attribute of endothelial progenitors and of hypoxic mature endothelial cells.* The Journal of the Federation of American Societies for Experimental Biology, 2012. **26**(12): p. 4925-4936.

[88] Santiago, J.-J., et al., *Cardiac Fibroblast to Myofibroblast Differentiation In Vivo and In Vitro: Expression of Focal Adhesion Components in Neonatal and Adult Rat Ventricular Myofibroblasts.* Developmental Dynamics, 2010. **239**: p. 1573-1584.

[89] Sugihara, A., et al., *Promotive effects of a silk film on epidermal recovery from full-thickness skin wounds.* Proceedings of the Society for Experimental Biology and Medicine, 2000. **225**(1): p. 58-64.

[90] Allmeling, C., et al., *Spider silk fibers in artificial nerve constructs promote peripheral nerve regeneration.* Cell Proliferation, 2008. **41**(3): p. 408-420.